Calculation of induced magnetic form factor of chromium

by

Kye Hwan Oh

A Dissertation Submitted to the
Graduate Faculty in Partial Fulfillment of
The Requirements for the Degree of
DOCTOR OF PHILOSOPHY

Department: Physics
Major: Solid State Physics

Approved:

Signature was redacted for privacy.

In Charge of Major Work

Signature was redacted for privacy.

For the Major Department

Signature was redacted for privacy.

For the Graduate College

Iowa State University
Ames, Iowa

1975

TABLE OF CONTENTS

CHAPTER I. INTRODUCTION

The object of this study is to determine the magnetization density of metallic chromium induced by an external magnetic field. For this purpose we attempted a realistic calculation of the susceptibility and the induced magnetic form factor by using the augmented plane wave (APW) energy bands and wavefunctions.

Magnetic form factor measurements, which determine the Fourier transform of the total magnetization density, have been used quite extensively for the study of the magnetic properties of solids. The magnetization density of a magnetic atom or ion is the sum of the spin density and the magnetic moment density due to the orbital motion of the electrons. This is analogous to the x-ray form factor which measures the charge density and describes the scattering of the electromagnetic waves by the entire electron cloud of the atom. By comparing these experimental results with the form factors obtained from detailed calculation, we hope to gain insight into the magnitude and character of the various contributions to the magnetization.

Measurements of the neutron magnetic form factor in the antiferromagnetic state were performed by Moon, Koehler and Trego[1] for a single crystal of Cr with small additions of Mn. The data were interpreted rather successfully using the simple atomic model[2] in which the magnetic spin density is assumed to have the same distribution as that calculated with free atom Hartree-Fock 3d electrons.

Asano and Yamashita,[3] in their calculation of paramagnetic and antiferromagnetic band structures of chromium, calculated the antiferromagnetic form factor which is mainly due to the uncompensated spins of conduction electrons. Their calculated form factor for the ordered state was in good agreement with the above measurements.

Recently Stassis, Klein and Sinha[4] have performed a neutron form factor measurement on the paramagnetic chromium by using the polarized neutron technique. The comparison of this paramagnetic neutron form factor with that of the ordered state[1] shows that the former decreases less rapidly than the latter as the scattering angle increases. This suggests that the induced magnetization density has a more contracted spatial distribution than the spin density in the ordered state. Stassis et al.[4] analyzed their data in terms of a simple atomic model which uses the 3d free ion form factors of Freeman and Watson,[2] and showed that an assumed 60% orbital and 40% spin contribution to the induced magnetic neutron form factor were needed to explain the experiments. This predicted a gyromagnetic ratio of 1.25 which is in good agreement with the value measured independently by the Einstein-de Haas experiment.[5] Such a remarkably large orbital contribution seems to be real. This experiment provided a strong motivation for the detailed calculation of the susceptibility and the magnetic form factor undertaken in this dissertation.

The forward scattering amplitude in the neutron form factor corresponds to the bulk susceptibility. We will consider this bulk

susceptibility first since this gives us a simple and more familiar picture for the mechanisms of magnetization in a solid.

For ordered states the magnetic moments arise mainly from the unpaired eiectron spins. However in a paramagnetic state each energy band is doubly degenerate with spin up and spin down states, and there is no net spin magnetic moment. But when a magnetic field is applied, the spin up and spin down bands are shifted in opposite directions by the interaction energy between the electron spin and the magnetic field. This causes a redistribution of the electrons and gives rise to a net spin magnetic moment. This is called Pauli spin paramagnetism.[6a,b]

Van Vleck showed that in atoms an orbital magnetic moment can be induced by a weak magnetic field and the resultant magnetization gives rise to a temperature independent susceptibility, which is called Van Vleck susceptibility.[6a,b] The importance of the Van Vleck type orbital contribution to the paramagnetism in metals has been pointed out by Kubo and Obata,[7] and Orgel.[8] They[7] showed that even when the orbital angular momentum is quenched by the crystalline field in a metal, an orbital magnetic moment can be induced by an external magnetic field, and the magnitude of this term was shown to be about the same order as that of the Pauli spin paramagnetism. Lomer[9] has estimated crudely the Van Vleck type orbital susceptibility of chromium by averaging the matrix elements utilizing the tight binding states along the high symmetry directions in the Brillouin zone.

Another contribution to the orbital susceptibility arises from the quantized orbital motions of the electrons under the presence of the

magnetic field. This motion produces a magnetization in such a direction that the induced magnetic field due to the magnetization is opposite to that of the applied field. This is called Landau-Peierls diamagnetism[10,11] and its magnitude can be shown to be one third of the Pauli spin paramagnetism for free electron metals.[6a,b] In addition to the above discussed three terms, there is another diamagnetic contribution to the bulk susceptibility, which is associated with the tendency of core electrons to shield themselves from an applied magnetic field. This can be calculated just as is done for the susceptibility of the free atoms.

The bulk susceptibility is the spatially averaged magnetization density over the whole crystal, whereas the neutron form factor is the Fourier transform of the magnetization density. The magnetic neutron form factor gives us more information on the magnetization density because it describes its spatial distribution. The neutron form factor in a paramagnetic state arises from the same mechanisms as the bulk susceptibility, namely, the induced spin magnetization (Pauli spin paramagnetism) and the induced orbital magnetization (Van Vleck paramagnetism, Landau-Peierls diamagnetism and the core diamagnetism).

In the course of the calculation of induced magnetization of chromium, we formulated the neutron magnetic form factor from first principles by using the linear response theory. Following is the preview of this study.

In Chapter ii, we define a Fourier transform of the induced magnetic current operator in the Dirac field. The expectation value of

this current operator is obtained by using the first order perturbation theory.

Associating this magnetic current with the induced magnetization of the electron due to an external field, we obtain an explicit expression for the induced magnetic form factor. This induced magnetic form factor will then be shown by using the Gordon decomposition to consist of two terms: (1) the induced spin form factor, which is due to the induced magnetization of electrons, and (2) the induced orbital form factor, which is induced by the orbital motion of the electrons. Each contribution is then studied nonrelativistically by keeping only the large components of the relativistic wavefunctions. The orbital form factor has been worked out in great detail to find that it consists of the Van Vleck type terms, the Landau-Peierls like terms and the core diamagnetic type terms.

Details of the theoretical background for computation are presented in Chapter III. This includes the review of the APW method and the presentation of explicit expressions of the spin form factor for Bloch electrons, and the current, and angular momentum operator matrix elements involved in the Van Vleck type orbital form factor. A technique for the k-space volume integration is also presented in this chapter. These computational techniques have been used for the numerical calculation of induced Pauli type spin and Van Vleck type orbital magnetic form factor of Cr. Numerical results and its comparision with experimental results[4] are presented in Chapter IV.

CHAPTER II. FIELD INDUCED NEUTRON MAGNETIC FORM FACTOR

Introduction

Recently many neutron magnetic form factors have been measured for the 3d transition metals. Most of these experimental results have been interpreted in terms of the free atom or ion form factors, which were calculated quite extensively by Freeman and Watson[2] using Hartree-Fock atomic wavefunctions. The reason for employing the atomic form factors is simply because form factor calculations for solids are very difficult to perform since one must use the crystal wavefunctions.

In the following section, we will review briefly the atomic model of the magnetic form factor, and in section 3 we will formulate an expression for the induced magnetic form factor from first principles using the linear response theory. Various contributions of the magnetic form factor, spin and orbital, will be studied in detail for Bloch electrons.

Extreme Tight-Binding Limit: Atomic Model

The differential cross section for the elastic magnetic scattering of unpolarized neutrons into solid angle $d\Omega$[12,13] is (in the Born approximation)

$$\frac{d\sigma}{d\Omega} = \left(\frac{\gamma e^2}{mc^2}\right)^2 \sum_{qq'} p_q \left| \sum_n e^{i\vec{K}\cdot\vec{n}} \langle q' \left| \vec{T}_n \right| q \rangle \right|^2 \qquad (1)$$

where $|q\rangle$ and $|q'\rangle$ are the initial and final states of the crystal which have the same energy eigenvalues, $\vec{K} = \vec{k} - \vec{k}'$ is the difference between the initial and final wave vectors, $\vec{k}$ and $\vec{k}'$, respectively, of the neutron

($|\vec{k}| = |\vec{k}'|$), $\vec{n}$ is a lattice vector, γ is the gyromagnetic ratio of the neutron, and p_q is the probability that the state $|q\rangle$ is occupied. The operator $\vec{T}_n$ represents the interaction of the neutron with the electrons of the atom at site $\vec{n}$, and is given by[12,13]

$$\vec{T}_n = \sum_j e^{i\vec{K}\cdot\vec{r}_j} \hat{K} \times (\vec{s}_j \times \hat{K}) - \frac{i}{\hbar K} \sum_j e^{i\vec{K}\cdot\vec{r}_j} (\hat{K} \times \vec{p}_j) \qquad (2)$$

where $\vec{s}_j$ and $\vec{p}_j$ are the spin and momentum of the j^{th} electron, $\vec{r}_j$ is the position of the electron relative to the lattice point $\vec{n}$, $\hat{K}$ is a unit vector in the direction of $\vec{K}$, and the summation is over all electrons of the atom at lattice site $\vec{n}$.

Analysis of the neutron form factor measurements with the atomic model are based on the following two assumptions: (1) The local magnetization density is solely due to the 3d electrons. This is a reasonable approximation because a large percentage of the conduction electrons, especially near the Fermi surface, are d-like (see Cr bands 3, 4 and 5 in Fig. 4). (2) The crystal wavefunctions both for spin up and spin down electrons have the same radial dependence as the free ions (if spin polarized wavefunctions are not available). Based on these assumptions, we impose a crystalline field on the atomic wavefunctions, which gives rise to a crystalline anisotropy. Degeneracies of the atomic wavefunctions are broken up according to the symmetry of the crystalline fields. In the cubic field, as an example, the five fold degenerate set of d wavefunctions splits into a triply degenerate set of T_{2g} orbitals, and a doubly degenerate set of E_g orbitals.

The spin part of the form factor Eq. (1) for the crystal field split levels, which is normalized to 1 at $\vec{K} = 0$, can be written as

$$f_{T_{2g}}(\vec{K}) = \int \psi^{*}_{T_{2g}} \psi_{T_{2g}} e^{i\vec{K}\cdot\vec{r}} d\vec{r}$$

$$= \langle j_0(Kr) \rangle - A\langle j_4(Kr) \rangle ,$$

and

$$f_{E_g}(\vec{K}) = \langle j_0(Kr) \rangle + \frac{3}{2} A \langle j_4(Kr) \rangle \qquad (3)$$

where A, which is related to directional cosines of the scattering vector $\vec{K}$, can be written in terms of the Miller indices, h k l, as

$$A = \frac{h^4 + k^4 + l^4 - 3(h^2k^2 + k^2l^2 + l^2h^2)}{(h^2 + k^2 + l^2)^2} ,$$

and

$$\langle j_\ell(Kr) \rangle = \int_0^\infty R^2(r)\, j_\ell(Kr)\, r^2\, dr \qquad (4)$$

with the appropriate atomic radial function R(r) and the spherical Bessel function $j_\ell(Kr)$.

The orbital magnetic form factor was first considered for the rare earth ions by Trammell,[14] and this was extended for the study of the nickel ion by Blume.[13] The orbital part of the magnetic form factor in Eq. (1) is very similar in form to the spin form factor and can be

obtained by simply replacing $\langle j_0 \rangle$ by $\langle g_0 - \frac{1}{2} g_2 \rangle$ and $\langle j_4 \rangle$ by $\langle \frac{3}{14} g_4 - \frac{1}{7} g_2 \rangle$ in the form factor in Eq. (3). The g_L functions are defined as

$$g_L(x) = \frac{2}{x^2} \int_0^x j_L(r)\, r\, dr \tag{5}$$

and numerical values of $\langle g_L \rangle$ can be obtained from $\langle j_L \rangle$'s. In the case of Cr, Stassis et al.[4] found that their induced magnetic form factor can be explained well with a 60% orbital and a 40% spin 3d ionic form factors as shown in Fig. 8.

In this way, the magnetic form factor measurements were interpreted rather well in terms of the free atom or in this case free ion form factors. It is somewhat surprising to have such a good agreement between the experimental results and the atomic or ionic form factors because the crystal wavefunctions have s and p character as well as d, and they have different radial dependence for different energies as in Fig. 9, and the crystal charge densities at the Fermi energy are more spread out than the atomic one as can be seen in Fig. 7.

Linear Response Theory for Crystal

Elastic neutron diffraction experiment for a paramagnetic crystal measures the induced moment scattering amplitude $P(\theta)$, which is proportional to the Fourier transform of the induced magnetization density $\langle \vec{M}(\vec{Q}) \rangle$ along the direction of external magnetic field $\vec{B}(\vec{Q})$:[4,15]

$$P(\theta) = (\mu_n r_0) \frac{1}{2\mu_B} \langle \vec{M}(\vec{Q}) \rangle . \tag{6}$$

Here $\mu_n = 1.91$ is the magnetic moment of the neutron in nuclear magnetons, r_0 is the classical electron radius $\frac{e^2}{mc^2}$, μ_B is the Bohr magneton, $\vec{Q}$ is the neutron scattering vector of magnitude $4\pi \sin\theta/\lambda$. λ is the wavelength, and 2θ is the scattering angle. In the following, we will study the susceptibility function $\chi(\vec{Q},\vec{q})$ which relates the magnetization density $\vec{M}(\vec{Q})$ with the applied magnetic field $B(\vec{q})$ via linear response theory.

In the presence of a magnetic field, a covariant form of the Dirac equation[16] for a central field can be written as

$$\left(\frac{\partial}{\partial x_\mu} - \frac{ie}{\hbar c} A_\mu\right) \gamma_\mu \psi + \frac{mc}{\hbar} \psi = 0 \tag{7}$$

where $x_\mu = (\vec{x}, ict)$ and $A_\mu = (\vec{A}(\vec{r}), iV(\vec{r})/e)$, and the γ_μ's are the Dirac matrices whose definitions can be found in the standard quantum mechanics texts.[16] The $\vec{A}(\vec{r})$ is the vector potential which is related with the magnetic field via the familiar relation

$$\vec{B}(\vec{r}) = \vec{\nabla} \times \vec{A}(\vec{r}) \ . \tag{8}$$

Within the framework of the single particle Dirac theory, the charge current density operator is defined by

$$J_\mu(\vec{r}) = iec\bar{\psi}\gamma_\mu\psi \ .$$

This becomes, in terms of the Fourier components,

$$J_\mu(\vec{Q}) = iec\bar{\psi}\gamma_\mu e^{-i\vec{Q}\cdot\vec{r}}\psi \equiv \psi^\dagger j_\mu(\vec{Q})\,\psi \tag{9}$$

where

$$j_\mu(\vec{Q}) = iec\gamma_4\gamma_\mu e^{-i\vec{Q}\cdot\vec{r}}, \tag{10}$$

and $\bar{\psi}$ is the adjoint wavefunction defined by $\psi^\dagger\gamma_4$. The physical meaning of the charge current density can be seen easily if J_μ is written in the following fashion,

$$J_\mu(\vec{Q}) = \frac{iec}{2}(\bar{\psi}\gamma_\mu e^{-i\vec{Q}\cdot\vec{r}}\psi + \bar{\psi}\gamma_\mu e^{-i\vec{Q}\cdot\vec{r}}\psi)$$

$$= \frac{ie\hbar}{2m}[-\bar{\psi}\gamma_\mu\gamma_\nu e^{-i\vec{Q}\cdot\vec{r}}(\frac{\partial}{\partial x_\nu} - \frac{ie}{\hbar c}A_\nu)\psi$$

$$+ \{(\frac{\partial}{\partial x_\nu} + \frac{ie}{\hbar c}A_\nu)\bar{\psi}\}\gamma_\nu\gamma_\mu e^{-i\vec{Q}\cdot\vec{r}}\psi] \tag{11}$$

where the summation convention was used. We now split $J_\mu(\vec{Q})$ in Eq. (11) into two parts according to whether or not the summation index ν coincides with μ. We then have

$$J_\mu = J_\mu^{(1)} + J_\mu^{(2)} \tag{12}$$

where

$$J_\mu^{(1)} = \frac{ie\hbar}{2m}(\frac{\partial\bar{\psi}}{\partial x_\mu}\psi\, e^{-i\vec{Q}\cdot\vec{r}} - \bar{\psi}\, e^{-i\vec{Q}\cdot\vec{r}}\frac{\partial\psi}{\partial x_\mu})$$

$$- \frac{e^2}{mc}A_\mu e^{-i\vec{Q}\cdot\vec{r}}\bar{\psi}\psi, \tag{13}$$

and

$$J_{\mu}^{(2)} = -\frac{e\hbar}{2m}\frac{\partial}{\partial x_{\nu}}(\bar{\psi}\,\sigma_{\nu\mu}\,\psi)\,e^{-i\vec{Q}\cdot\vec{r}} \tag{14}$$

The current density, namely, 1,2,3 components of the charge-current density Eq. (12), can be written after a few manipulations as

$$\vec{J}(\vec{Q}) = \bar{\psi}\vec{j}_{tot}(\vec{Q})\psi - \frac{e^2}{mc}\bar{\psi}\vec{A}(\vec{r})\,e^{-i\vec{Q}\cdot\vec{r}}\psi \tag{15}$$

where

$$\vec{j}_{tot}(\vec{Q}) = \vec{j}_{orb}(\vec{Q}) + \vec{j}_{spin}(\vec{Q}) = iec\gamma_4\vec{\gamma}\,e^{-i\vec{Q}\cdot\vec{r}} \tag{16}$$

with

$$\vec{j}_{orb}(\vec{Q}) = \frac{e}{2m}(\vec{p}\,e^{-i\vec{Q}\cdot\vec{r}} + e^{-i\vec{Q}\cdot\vec{r}}\vec{p}), \tag{17}$$

$$\vec{j}_{spin}(\vec{Q}) = \frac{ie\hbar}{2m}\vec{Q}\times\vec{\sigma}\,e^{-i\vec{Q}\cdot\vec{r}} \tag{18}$$

This decomposition of the current density in Eq. (15) clearly shows that the current density is composed of two contributions, namely, (1) orbital current which is due to the moving electron charges, thus solely related with the orbital motion of electrons, and (2) the spin current which is associated with the magnetization of electrons. This separation is well known and is called Gordon decomposition.[16]

Now we obtain the expectation value of the current operator by utilizing the perturbation theory, where the total wavefunction ψ in

Eq. (7) is expanded in terms of the unperturbed wavefunctions assuming the applied magnetic field is weak. The field dependent Hamiltonian in Eq. (7) can be seen more clearly if we write the Dirac Hamiltonian in terms of the $\vec{\alpha}$ and β Dirac matrices[16] as

$$H = c\vec{\alpha} \cdot (\vec{p} - \frac{e}{c}\vec{A}(\vec{r})) + \beta mc^2 + V(r) \tag{19}$$

$$\equiv H_0 + H_1$$

where

$$H_o = c\vec{\alpha} \cdot \vec{p} + \beta mc^2 + V(r) \ , \tag{20}$$

$$H_1 = - e\vec{\alpha} \cdot \vec{A}(\vec{r}) \ . \tag{21}$$

The perturbing Hamiltonian H_1 will be written again in terms of the Fourier components as

$$H_1 = - \frac{i}{c} [\vec{A}(\vec{q}) \cdot \vec{j}^{\dagger}_{tot}(\vec{q}) + \vec{A}^{\dagger}(\vec{q}) \cdot \vec{j}_{tot}(\vec{q})] \ . \tag{22}$$

If we keep only the linear terms in the field, the wavefunction which is normalized within the first order of perturbation becomes

$$\psi = |n\rangle + \sum_m{}' f_n(1 - f_m) \frac{\langle m | H_1 | n \rangle}{E_n - E_m} |m\rangle \ , \tag{23}$$

with

$$H_o |n\rangle = (E_n + mc^2) |n\rangle \quad \text{and} \quad \langle m|n\rangle = \delta_{m,n} \tag{24}$$

where the unperturbed states $|n\vec{sk}\rangle$ with band index n, electron spin s and the crystal momentum $\vec{k}$ were abbreviated with $|n\rangle$. Note that the Fermi-Dirac distribution functions were included explicitly to show the allowed transitions, and the E_n's in Eqs. (23) and (24) are the band energies. A straightforward application of the wavefunction of Eq. (23) to the current density Eq. (15) gives us the expectation value of the current operator

$$\langle \vec{J}(\vec{Q}) \rangle = \frac{1}{c} \sum_{nm}' \frac{f_m - f_n}{E_n - E_m} \langle n | \vec{j}_{tot}(\vec{Q}) | m \rangle \langle m | \vec{A}(\vec{q}) \cdot \vec{j}^{\dagger}_{tot}(\vec{q})$$

$$+ \vec{A}^{\dagger}(\vec{q}) \cdot \vec{j}_{tot}(\vec{q}) | n \rangle$$

$$- \frac{e^2}{mc} \sum_n f_n \langle n | \vec{A}(\vec{q}) e^{i(\vec{q}-\vec{Q})\cdot\vec{r}} + \vec{A}^{\dagger}(\vec{q}) e^{-i(\vec{q}+\vec{Q})\cdot\vec{r}} | n \rangle \qquad (25)$$

where the expectation value of $\vec{J}(\vec{Q})$ in the ground states was not shown because it is zero.

The induced magnetization $\vec{M}$ which is associated with this magnetic current can be deduced from Eq. (25) considering the relation

$$\vec{J}(\vec{r}) = c\ \vec{\nabla} \times \vec{M}(\vec{r}) , \qquad (26)$$

or

$$\vec{M}(\vec{Q}) = \frac{i}{cQ^2}\ \vec{Q} \times \vec{J}(\vec{Q}) \qquad (27)$$

in terms of the Fourier components. In Eq. (27) , we considered that, as was in Eq. (6), $\vec{M}(\vec{Q})$ ia parallel to the direction of $\vec{B}(\vec{Q})$ which is perpendicular to $\vec{Q}$.

Together with Eqs. (25) and (27), the linear response theory in which the induced magnetization is related with $\vec{B}$ by

$$\langle M_i(\vec{Q})\rangle = \sum_j [\chi_{ij}(\vec{Q},\vec{q})B_j(\vec{q}) + \chi_{ij}(\vec{Q},-\vec{q})B_j^*(\vec{q})] , \tag{28}$$

enables us to write down the explicit expression for the linear response function χ_{ij},

$$\chi_{ij}(\vec{Q},\vec{q}) = \frac{1}{c^2q^2Q^2}\sum_{nm}\frac{f_n-f_m}{E_n-E_m}\langle n|(\vec{Q}\times\vec{j}_{tot}(\vec{Q}))_i|m\rangle\langle m|(\vec{q}\times\vec{j}_{tot}^{\dagger}(\vec{q}))_j|n\rangle$$

$$-\frac{e^2}{mc^2q^2Q^2}[(\vec{q}\cdot\vec{Q})\delta_{ij} - q_iQ_j]\sum_n\langle n|e^{i(\vec{q}-\vec{Q})\cdot\vec{r}}|n\rangle \tag{29}$$

where the integrations are to be performed over the whole crystal. From now on, we will keep only the large components among the four component wavefunctions which are involved in the matrix elements in Eq. (29). No confusion should be made for the wavefunctions which appear in the following. They are nonrelativistic wavefunctions.

The z axis of the system will be chosen along the direction of the applied magnetic field $\vec{B}$. With this choice of z axis, we take the directions of the scattering vector $\vec{Q}$ and the wave vector of the field $\vec{q}$ to be parallel and pointing along the y axis. This choice of $\vec{Q}$ direction can always be obtained because the neutron diffraction experiment measures the reflections on the x-y plane, and thus we are free to rotate the system about the z axis to place $\vec{Q}$ along the y axis.

Under the uniform applied field $\vec{q}\to 0$, we can obtain the relationship between the induced moment scattering amplitude P(θ) of Eq. (6)

and the susceptibility function $\chi_{zz}(\vec{Q},0)$ using the linear response of Eq. (28), which is

$$P(\theta) = (\mu_n r_0) \frac{B}{\mu_B} \chi_{zz}(\vec{Q},0). \tag{30}$$

The integrals over the whole crystal volume involved in Eq. (29) will now be reduced to the integrals over the unit cell volume by using the periodic nature of Bloch wavefunctions. This Bloch condition also requires that $\vec{Q} - \vec{q}$ should be the same as the reciprocal lattice vectors. Then the neutron magnetic form factor can be written as

$$\lim_{q\to 0} \chi_{zz}(G+q, q) =$$

$$\lim_{q\to 0} \Big[\frac{2e^2}{m^2c^2(G+q)q} \sum_{\substack{nk \\ n'k'}} \frac{f_{nk} - f_{n'k'}}{E_{n'k'} - E_{nk}} \langle n\vec{k}|p_x e^{-i(G+q)y}|n'\vec{k}'\rangle$$

$$\times \langle n'\vec{k}'|p_x e^{iqy}|n\vec{k}\rangle$$

$$- 2\left(\frac{e\hbar}{2mc}\right)^2 \sum_{\substack{nk \\ n'k'}} \frac{f_{nk} - f_{n'k'}}{E_{n'k'} - E_{nk}} \langle n\vec{k}|e^{-i(G+q)y}|n'\vec{k}'\rangle \langle n'\vec{k}'|e^{iqy}|n\vec{k}\rangle$$

$$- \frac{2e^2}{mc^2(G+q)q} \sum_{nk} f_{nk} \langle n\vec{k}|e^{iGy}|n\vec{k}\rangle\Big] \tag{31}$$

where $\vec{Q} = \vec{G} + \vec{q}$ and $\vec{q}$ along the y direction, and the $\vec{M}$ and $\vec{B}$ along the z direction. In the above expression a spin orientation factor of 2 was included, and the band index n and the crystal momentum $\vec{k}$ were introduced explicitly for the wavefunction representation. Note that

if the radial functions for spin up and spin down states change appreciably as the spin degeneracy of bands are removed, the cross terms between the spin and the orbital currents in Eq. (29) would contribute to the form factor, which is of the order of spin orbit coupling. However since we are presently concerned with the paramagnetic states, the radial functions of the spin up and spin down states do not split appreciably under the perturbing Hamiltonian, and thus the sum over spins in Eq. (29) gives no such cross terms in the paramagnetic state.

In the Appendix, we proved that there are no q^{-1} divergent terms in Eq. (31) as q goes to zero. Then we finally obtain a simplified form of the magnetic form factor $\chi_{zz}(G,0)$ after leaving out the q^{-1} divergent terms from Eq. (31), which can be written as

$$\chi_{zz}(G,0) = \chi_{zz}^{spin}(G,0) + \chi_{zz}^{orbit}(G,0)$$

where

$$\chi_{zz}^{spin}(G,0) = \lim_{q\to 0}\Big[-2\left(\frac{e\hbar}{2mc}\right)^2 \sum_{nn'k} \frac{f_{nk} - f_{n'k+q}}{E_{n'k+q} - E_{nk}} \times \langle n\vec{k}|e^{-i(G+q)y}|n'\vec{k}+\vec{q}\rangle \langle n'\vec{k}+\vec{q}|e^{iqy}|n\vec{k}\rangle \Big] \qquad (32)$$

$$= 2\left(\frac{e\hbar}{2mc}\right)^2 \sum_{\substack{n\vec{k} \\ E=E_F}} \frac{\Delta S_n(\vec{k})}{|\nabla_K E_n(\vec{K})|_{\vec{K}=\vec{k}}} \langle n\vec{k}|e^{-iGy}|n\vec{k}\rangle \qquad (32')$$

and

$$\chi_{zz}^{orbit}(G,0) = \lim_{q\to 0} \frac{\partial}{\partial q}\left[\frac{2e^2}{m^2c^2G} \sum_{nn'k} \frac{f_{nk} - f_{n'k+q}}{E_{n'k+q} - E_{nk}}\right.$$

$$\left. \times \langle n\vec{k}| p_x e^{-i(G+q)y} |n'\vec{k}+\vec{q}\rangle \langle n'\vec{k}+\vec{q}| p_x e^{iqy} |n\vec{k}\rangle\right] , \qquad (33)$$

where $\Delta S_n(\vec{k})$ are the surface elements for the constant energy surface at the Fermi energy E_F. The states involved in the spin form factor should be those near $E = E_F$ due to the Fermi distribution functions in the numerator of Eq. (32). From now on we will study the spin and orbital magnetic form factors separately using the explicit expressions of Bloch wavefunctions.

Spin form factor

It is interesting to see that the spin part of the form factor Eq. (32') leads to the Pauli spin susceptibility[6a,b] at $G = 0$,

$$\chi_{Pauli} = 2\left(\frac{e\hbar}{2mc}\right)^2 \sum_{\substack{n\vec{k} \\ E_n = E_F}} \frac{\Delta S_n(\vec{k})}{|\nabla_k E_n(\vec{k})|}$$

$$= \mu_B^2 \, D(E_F) \qquad (34)$$

where μ_B is the Bohr magneton $\frac{e\hbar}{2mc}$, and $D(E_F)$ is the density of states at the Fermi energy defined[17] as

$$D(E_F) = 2 \sum_{\substack{n\vec{k} \\ E_n=E_F}} \frac{\Delta S_n(\vec{k})}{|\nabla_k E_n(\vec{k})|}$$

$$= \frac{2\Omega}{(2\pi)^3} \int_{E=E_F} \frac{dS}{|\nabla_k E(\vec{k})|} \, . \tag{35}$$

where a factor 2 is for the two spin orientations. We know that this Pauli spin susceptibility is due to a magnetic field which breaks the degeneracy of the electrons of opposite spins that share the same orbital state. In a metal this causes the electrons near the Fermi surface to redistribute and give rise to a magnetic moment, which is essentially temperature independent.

For the calculation of the induced magnetic spin form factor for G other than zero, it is very convenient to write the χ_{zz}^{spin} in Eq. (32) as

$$\chi_{zz}^{spin}(\vec{G},0) = \int_{cell} \rho(\vec{r}) \, e^{-i\vec{G}\cdot\vec{r}} d\vec{r} \, , \tag{36}$$

where

$$\rho(\vec{r}) = \mu_B^2 \sum_{\substack{n\vec{k} \\ E=E_F}} \frac{\Delta S_n(\vec{k})}{|\nabla_{\vec{k}} E_n(\vec{k})|} \, \varphi^*_{n\vec{k}}(\vec{r}) \varphi_{n\vec{k}}(\vec{r}) \tag{37}$$

is the properly weighted average crystal charge density of orbits at the the Fermi energy. Details of the spin form factor for the Bloch wavefunctions are presented in Chapter III.

Orbital form factor

The contributions to the orbital form factor can be divided into two parts according to the dependence of the matrix elements on $\vec{q}$. Terms arising from the q independent matrix elements are called Landau terms because at $\vec{G}=0$ its intraband contributions give rise to the Landau diamagnetic susceptibility[10] in the free electron limit, and the others are called non-Landau terms. In the following, we will obtain the explicit expressions for these contributions.

First, Landau contributions will be collected from Eq. (33). These are (1) intraband Landau terms ($n=n'$),

$$\chi_L^{intra}(G,0) = \frac{2e^2}{m^2c^2G} \sum_{nk} \left[-\frac{i}{2}\frac{\partial E_{nk}}{\partial k_y} \right] \frac{\partial^2 f_{nk}}{\partial E_{nk}^2}$$

$$\times \langle n\vec{k}| p_x e^{-iGy} |n\vec{k}\rangle \langle n\vec{k}| p_x |n\vec{k}\rangle \qquad (38)$$

where we used

$$f_{nk} - f_{n,k+q} = f(E_{nk}) - f(E_{n,k+q})$$

$$= (E_{nk} - E_{nk+q})\frac{\partial f(E_{nk})}{\partial E_{nk}} + \frac{1}{2}(E_{nk} - E_{nk+q})^2 \frac{\partial^2 f(E_{nk})}{\partial E_{nk}^2} + \cdots \qquad (39)$$

and

$$E_{nk+q} - E_{nk} = q \frac{\partial E_{nk}}{\partial k_y} + \frac{1}{2} q^2 \frac{\partial^2 E_{nk}}{\partial k_y^2} + \cdots \tag{40}$$

(2) interband Landau terms ($n \neq n'$),

$$\chi_L^{inter}(G,0) = \frac{2e^2}{m^2 c^2 G} \sum_{nk} \sum_{n' \neq k} \left[\frac{f_{nk} - f_{n'k}}{(E_{n'k} - E_{nk})^2} \left(- \nabla_{k_y} E_{n'k} \right) + \frac{1}{E_{n'k} - E_{nk}} \right.$$

$$\left. \times \left(- \frac{\partial f_{n'k}}{\partial k_y} \right) \right] \times \langle n\vec{k} | p_x e^{-iGy} | n'\vec{k} \rangle \langle n'\vec{k} | p_x | n\vec{k} \rangle \tag{41}$$

where we used

$$\frac{1}{E_{n'k+q} - E_{nk}} = \frac{1}{E_{n'k} - E_{nk}} - q(\nabla_{k_y} E_{n'k}) \frac{1}{(E_{n'k} - E_{nk})^2} + \cdots \tag{42}$$

and

$$f_{nk} - f_{n'k+q} = f_{nk} - f_{n'k} - q \frac{\partial f_{n'k}}{\partial k_y} - \cdots \tag{43}$$

The non-Landau terms can be written as

$$\chi_{NL}(G,0) = \frac{2e^2}{m^2 c^2 G} \sum_{nn'k} \frac{f_{nk} - f_{n'k}}{E_{n'k} - E_{nk}} \left[\langle u_{nk} | (p_x + \hbar k_x) e^{-iGy} | \nabla_{k_y} u_{n'k} \rangle \right.$$

$$\times \langle u_{n'k} | p_x + \hbar k_x | u_{nk} \rangle + \langle u_{nk} | (p_x + \hbar k_x) e^{-iGy} | u_{n'k} \rangle \times$$

$$\left. \langle \nabla_{k_y} u_{n'k} | p_x + \hbar k_x | u_{nk} \rangle \right] \tag{44}$$

where we wrote the wavefunctions in Eq. (33) in terms of the explicit form of Bloch states

$$|n\vec{k}\rangle = e^{i\vec{k}\cdot\vec{r}} u_{nk}(\vec{r}) \tag{45}$$

with periodic wavefunctions $u_{nk}(\vec{r})$. If we substitute the following identities into the above equation (44),

$$\nabla_k u_{nk} = -i\vec{r}u_{nk} + i\langle n\vec{k}|\vec{r}|n\vec{k}\rangle + \frac{i\hbar^2}{2m} \sum_{n'\neq n} \frac{S_{n'nk}(\vec{r})}{E_{nk} - E_{n'k}} u_{n'k} , \tag{46}$$

with

$$S_{n'nk}(\vec{r}) = \int_{\substack{\text{unit cell}\\ \text{surface}}} d\vec{s} \cdot [\nabla \varphi^*_{n'k} \vec{r} \varphi_{nk} - \varphi^*_{n'k} \nabla(\vec{r}\varphi_{nk})] , \tag{47}$$

and

$$p_x y = -\frac{1}{2} L_z + \frac{1}{2} (p_x y + x p_y) \text{ etc,} \tag{48}$$

Eq. (44) becomes

$$\chi_{NL}(G,0) = -\frac{ie^2}{mc^2 G} \sum_n f_{nk} \langle n\vec{k}|ye^{-iGy}|n\vec{k}\rangle$$

$$-\frac{ie^2}{m^2c^2G} \sum_{nn'k} \frac{f_{nk} - f_{n'k}}{E_{n'k} - E_{nk}} \langle n\vec{k}|p_x e^{-iGy}|n'\vec{k}\rangle \langle n'\vec{k}|L_z|n\vec{k}\rangle$$

$$+\frac{e^2\hbar}{m^2c^2G} \sum_{nn'k} \frac{f_{nk} - f_{n'k}}{E_{n'k} - E_{nk}} [\langle n\vec{k}|p_x y e^{-iGy}|n'\vec{k}\rangle S_{n'nk}(x)$$

$$-\frac{1}{2}\langle n\vec{k}|p_x e^{-iGy}|n'\vec{k}\rangle S_{n'nk}(xy) + \frac{\hbar}{m}\sum_{n'\neq n''}\frac{1}{E_{n'k}-E_{n''k}}\{\langle n'\vec{k}|p_x|n\vec{k}\rangle S_{n''n'k}(y)$$

$$x\langle n\vec{k}|p_x e^{-iGy}|n''\vec{k}\rangle + \langle n\vec{k}|p_x e^{-iGy}|n'\vec{k}\rangle S^{*}_{n''n'k}(y)\langle n''\vec{k}|p_x|n\vec{k}\rangle\}] \quad . \tag{49}$$

The first term in above expression can be identified as part of the core diamagnetic form factor, the second term is to be identified with the Van Vleck like contributions, and the last with surface terms. In order to see the Van Vleck like terms explicitly, we will further explore the second term in Eq. (49). This second term becomes as G approaches zero,

$$\lim_{G\to 0} -\frac{ie^2}{m^2c^2G}\sum_{nn'k}\frac{f_{nk}-f_{n'k}}{E_{n'k}-E_{nk}}\langle n\vec{k}|p_x(1-iGy+\cdots)|n'\vec{k}\rangle\langle n'\vec{k}|L_z|n\vec{k}\rangle$$

$$= \lim_{G\to 0} -\frac{ie^2}{m^2c^2G}\sum_{nn'k}\frac{f_{nk}-f_{n'k}}{E_{n'k}-E_{nk}}\langle n\vec{k}|p_x|n'\vec{k}\rangle\langle n'\vec{k}|L_z|n\vec{k}\rangle$$

$$-\frac{e^2}{m^2c^2}\sum_{nn'k}\frac{f_{nk}-f_{n'k}}{E_{n'k}-E_{nk}}\langle n\vec{k}|p_x y|n'\vec{k}\rangle\langle n'\vec{k}|L_z|n\vec{k}\rangle \tag{50}$$

The first term in Eq. (50) can be shown to be the first term of Eq. (49) with opposite sign except the surface terms. When we apply Eq. (48) to Eq. (50), the terms arising from the second part of Eq. (48) vanishes due to the odd symmetry. Finally the remainder of Eq. (50) is

$$2\mu_B^2\sum_{nn'k}\frac{f_{nk}-f_{n'k}}{E_{n'k}-E_{nk}}|\langle n\vec{k}|L_z|n'\vec{k}\rangle|^2 \quad . \tag{51}$$

It is interesting to see that Eq. (51) is the Van Vleck paramagnetic susceptibility, which arises from lowering the energies of occupied electron states due to the perturbing interaction Hamiltonian $-\mu_B \vec{B} \cdot \vec{L}$. It is this second term of Eq. (49) that we used for the calculation of the orbital magnetic form factor, which we call the Van Vleck type orbital form factor.

CHAPTER III. THEORETICAL BACKGROUND FOR COMPUTATION

The Augmented Plane Wave (APW) Method

The one electron model has been used successfully for the calculation of the electronic band structures of the transition metals. The essence of this model is to reduce the many electron problem to that of a single electron in the field of an effective crystal potential $V(\vec{r})$, where the corresponding Schrödinger equation in atomic units is

$$[- \nabla^2 + V(\vec{r})] \varphi(\vec{r}) = E \varphi(\vec{r}) \tag{52}$$

We assume $V(\vec{r})$ has a periodicity of the lattice, hence, with any translational vector $\vec{r}_s$,

$$V(\vec{r} + \vec{r}_s) = V(\vec{r}) \ . \tag{53}$$

Of the many methods available to solve this equation, the augmented plane wave (APW) and the Green's function (or KKR) methods seem to be the most accurate and the most rapidly convergent. We use the former in the form devised by Slater[18] and recently modified by Koelling[19] using the linearized method.

In the APW method we use a muffin-tin potential approximation, in which the unit cell is separated into two regions by nonoverlapping spheres surrounding each atomic site. Inside each sphere the potential is assumed to be spherically symmetric, and outside the spheres the potential is taken to be constant. It is then natural to choose a trial wavefunction in terms of a linear combination of the atomic-like wave-

functions for regions near the atomic sites, and in terms of the plane waves for regions away from the atomic sites. In the present study, however, we avoided the muffin-tin approximation in the interstitial region by using the actual potential (the so-called warped potential). The description of this warped potential is described in the next section. Since there have been a few excellent reviews of the APW method,[20,21] only those important aspects of obtaining the energy bands and wavefunctions will be given here. Before this we will first discuss briefly how the crystal potential of chromium was constructed.

The crystal potential

Chromium has an atomic configuration of $1s^1 2s^2 2p^6 3s^2 3p^6 3d^5 4s^1$, and forms a body centered cubic lattice in the crystal with a lattice constant 5.451 au.[22] A crystal potential is constructed in a manner which was first suggested by Mattheiss.[23] The atomic Coulomb potential is generated with the Hartree-Fock-Slater atomic charge densities which were obtained for the above atomic configuration. We use then the Löwdin alpha expansion to superpose the atomic Coulomb potential to construct a spherically symmetric Coulomb potential inside the muffin-tin sphere of radius r_{MT} = 2.326 au.

For chromium the atomic Coulomb potential from the nearest 15C lattice sites were summed to construct the crystal Coulomb potential. The atomic charge densities were again superposed in a similar manner to obtain a crystal charge density $\rho(r)$. Then we obtain the exchange potential by using Slater's free electron exchange approximation[24]

$$V_{ex}(r) = -6\left(\frac{3}{8\pi}\ \rho(r)\right)^{1/3} \tag{54}$$

This exchange potential was added to the crystal Coulomb potential to have a total crystal potential inside the muffin-tin sphere. For regions outside this sphere a warped potential instead of a flat one was created because, as pointed out by Harmon,[25] the angular dependence of the wavefunctions is found to be sensitive to the potential outside the muffin-tin spheres. The warped potential in the interstitial region was generated in the same way as the spherical potential inside the muffin-tin sphere, but it is expanded in terms of the symmetrized plane waves $S_{\vec{K}_n}(\vec{r})$ as

$$V(\vec{r}) = \sum_{\vec{K}_n} C(\vec{K}_n)\, S_{\vec{K}_n}(\vec{r}) \tag{55}$$

where

$$S_{\vec{K}_n}(\vec{r}) = \frac{1}{g}\sum_{\alpha=1}^{g} e^{i\alpha\vec{K}_n\cdot\vec{r}}\ . \tag{56}$$

In the above expression g is the number of group operations α, 48 for the cubic symmetry, and $\vec{K}_n$ are the reciprocal lattice vectors. The reason for this Fourier series type expansion of the warped potential is to obtain the matrix elements of the crystal potential with ease between the APW basis wavefunctions. These matrix elements are to be used later in the secular equation.

Secular equations in APW method

As mentioned in the previous section, we expand the crystal wavefunction inside a unit cell as

$$\varphi_{\vec{k},E}(\vec{r}) = \sum_i A_i(\vec{k},E)\, \chi_{\vec{k}_i}(\vec{r}) \tag{57}$$

where

$$\chi_{\vec{k}_i}(\vec{r}) = \frac{1}{\sqrt{\Omega}} e^{i\vec{k}_i \cdot \vec{r}}, \quad r \geq r_{MT} \tag{58}$$

$$= \sum_{\ell m} b_{\ell m} R_{\ell,E}(r)\, Y_{\ell m}(\hat{r}), \quad r \leq r_{MT}. \tag{59}$$

The sum in Eq. (57) is over a set of reciprocal lattice vectors $\vec{K}_i$. The $\vec{k}_i$'s above are shorthand for $\vec{k}+\vec{K}_i$ and Ω in Eq. (58) is the volume of a unit cell, and the function $R_{\ell,E}(r)$ is the solution of the radial Schrödinger equation with energy E,

$$\left[\frac{1}{r^2}\frac{d}{dr}\left(r^2\frac{d}{dr}\right) + \left\{E - V(r) - \frac{\ell(\ell+1)}{r^2}\right\}\right] R_{\ell,E}(r) = 0. \tag{60}$$

The $b_{\ell m}$ in Eq. (59) is chosen such that the basis functions in Eqs. (58) and (59) are continuous at the surface of the muffin-tin sphere, namely,

$$b_{\ell m} = 4\pi i^{\ell} Y^*_{\ell m}(\hat{k})\, j_{\ell}(k_i r_{MT}) / R_{\ell,E}(r_{MT}), \tag{61}$$

where we used the plane wave expansion[26]

$$e^{i\vec{k}\cdot\vec{r}} = 4\pi \sum_{\ell m} i^{\ell} j_{\ell}(kr)\, Y_{\ell m}(\hat{r})\, Y^*_{\ell m}(\hat{k}). \tag{62}$$

Notice that the slope of the resulting wavefunction still remains discontinuous unless we choose an infinite number of basis functions, which is not possible in practice. We will now determine the expansion

coefficients A_i by using the Rayleigh-Ritz variational principle.

Schlosser and Marcus[27] have shown a variational expression which is valid for a trial wavefunction with a discontinuous slope on an arbitrary surface in the unit cell. This can be written for our muffin-tin sphere as

$$E \int_{I+II} \varphi^* \varphi \, d\vec{r} = \int_{I+II} \varphi^* H \varphi \, d\vec{r}$$

$$- \frac{1}{2} \int_{\text{surface}} (\varphi_{II}^* + \varphi_I^*)\left(\frac{\partial}{\partial r}\varphi_{II} - \frac{\partial}{\partial r}\varphi_I\right) ds \qquad (63)$$

where the regions for inside and outside the muffin-tin sphere were denoted by I and II, and the wavefunctions by φ_I and φ_{II} respectively, and $\frac{\partial}{\partial r}$ is in the direction of the outward normal for region I. Note that the second term on the right hand side of Eq. (63) arises from the slope discontinuity of the wavefunctions on the boundary.

Now, with the substitution of Eq. (57) into Eq. (63), a variational calculation can be performed by minimizing this expression with respect to the parameter A_i. If the energy eigenvalues E' for $\varphi_{k,E'}(\vec{r})$ are assumed to correspond to E of the stationary states of the system, we can show after the minimization that Eq. (63) reduces to a set of linear simultaneous equations

$$\sum_j \left[(\vec{k}_i \cdot \vec{k}_j - E)\, S(\vec{K}_j - \vec{K}_i) + \sum_n C(\vec{K}_n)\left\{\frac{1}{g}\sum_{\alpha=1}^{g} S(\vec{K}_j - \vec{K}_i + \alpha\vec{K}_n)\right\}\right.$$

$$\left. + \frac{4\pi r_{MT}^2}{\Omega} \sum_\ell (2\ell+1) P_\ell(\hat{k}_i \cdot \hat{k}_j)\, j_\ell(k_i r_{MT}) R'_{\ell E}(r_{MT}) / R_{\ell E}(r_{MT})\right] A_j = 0 \qquad (64)$$

where the second term in the bracket comes from the warped potential and the overlap integral between the plane waves $S(\vec{K}_j - \vec{K}_i)$ can be written as

$$S(\vec{K}_j - \vec{K}_i) = \frac{1}{\Omega} \int_{\text{out}} e^{i(\vec{K}_j - \vec{K}_i)\cdot\vec{r}} \, d\vec{r}$$

$$= \delta_{ij} - \frac{4\pi r_{MT}^2}{\Omega} \frac{j_1(|\vec{K}_j - \vec{K}_i| r_{MT})}{|\vec{K}_j - \vec{K}_i|} \quad . \tag{65}$$

We know from the elementary matrix analysis that a nontrivial solution for Eq. (64) exists if and only if its secular determinant vanishes. Finally this enables us to obtain a dispersion relation between E and $\vec{k}$. We can also obtain the plane wave expansion coefficients A_i by the back transformation.

Spin Form Factor with APW Wavefunctions

In this section we will study the details of the spin form factor of Eq. (36) in conjunction with the APW wavefunctions described in the previous section.

The Bloch wavefunctions of Eq. (57) which are obtained by the APW method can be written again as

$$\varphi_{\vec{k},E}(\vec{r}) = \sum_n A_n(\vec{k},E) \, e^{i(\vec{k}+\vec{K}_n)\cdot\vec{r}} \quad , \; r \geq r_{MT}$$

$$= \sum_{\ell m} A_{\ell m}(\vec{k},E) \, R_{\ell,E}(r) \, Y_{\ell m}(\hat{r}) \quad , \; r \leq r_{MT} \; . \tag{66}$$

where

$$A_{\ell m}(\vec{k},E) = 4\pi i^{\ell} \sum_{n} j_{\ell}(k_n r_{MT}) Y^{*}_{\ell m}(\hat{k}_n) A_n \ . \tag{67}$$

The plane wave expansion coefficients $A_n(\vec{k},E)$ are obtained first from the APW method, and $A_{\ell m}$'s are generated from A_n's via the relation (67).

For outside the muffin-tin sphere, the charge density in Eq. (37) can be written in terms of the symmetrized plane waves as

$$\rho_{out}(\vec{r}) = \sum_{\vec{K}_s} C(\vec{K}_s) S_{\vec{K}_s}(\vec{r}) \tag{68}$$

where $\vec{K}_s$'s are the representative reciprocal lattice vector for the stars, and

$$S_{\vec{K}_s}(\vec{r}) = \frac{1}{48} \sum_{\alpha=1}^{48} e^{-i\alpha\vec{K}_s \cdot \vec{r}} \tag{69}$$

is a symmetrized plane wave, and the α sum is for the operations of the space group (48 in the cubic symmetry).

For inside the muffin-tin sphere, the wavefunctions are in terms of the angular momentum states and we can rewrite the charge density in terms of the lattice harmonics $Z_L(\hat{r})$,

$$\rho_{in}(\vec{r}) = \sum_{L} C_L(r) Z_L(\hat{r}). \tag{70}$$

The lattice harmonics for the cubic structure can be written in terms of the usual spherical harmonics $Y_{\ell m}(\hat{r})$ as

$$Z_0 = Y_{00} ,$$

$$Z_4 = \sqrt{\frac{7}{12}}\, Y_{40} + \sqrt{\frac{5}{24}}\, (Y_{44} + Y_{4-4}) ,$$

$$Z_6 = \frac{\sqrt{2}}{4}\, Y_{60} - \frac{\sqrt{7}}{4}\, (Y_{64} + Y_{6-4}) . \tag{71}$$

The expansion coefficients $C_L(r)$ in Eq. (70) can be obtained easily by using the APW wavefunctions

$$C_L(r) = \sum_{\substack{\ell m \\ \ell' m'}} A^*_{\ell m}(\vec{k}) A_{\ell' m'}(\vec{k})\, R_{\ell, E_F}(r)\, R_{\ell', E_F}(r)$$

$$\times \int Y^*_{\ell' m'}(\hat{r})\, Z_L(\hat{r})\, Y_{\ell m}(\hat{r})\, d\Omega \tag{72}$$

Using these charge densities inside and outside the muffin-tin sphere, the induced magnetic spin form factor can be written in a calculable form as

$$\chi^{spin}_{zz}(\vec{G},0) = \int_{in} \rho_{in}(\vec{r})\, e^{-i\vec{G}\cdot\vec{r}} d\vec{r} + \int_{out} \rho_{out}(\vec{r})\, e^{-i\vec{G}\cdot\vec{r}} d\vec{r}$$

$$\equiv F_{in}(\vec{G}) + F_{out}(\vec{G}) \tag{73}$$

where

$$F_{in}(\vec{G}) = \sum_L 4\pi i^L Z_L(\hat{G}) \int_0^{r_{MT}} C_L(r)\, j_L(Gr) r^2 dr ,$$

$$F_{out}(\vec{G}) = C(\vec{K}_s)\,\frac{\Omega}{48}\sum_{\alpha=1}^{48}\delta(\vec{G}-\alpha\vec{K}_s)$$

$$-\sum_{\vec{K}_s} C(\vec{K}_s)\,\frac{\Omega}{48}\sum_{\alpha=1}^{48}\frac{4\pi r_{MT}^2\, j_1(|\vec{G}-\alpha\vec{K}_s|\, r_{MT})}{|\vec{G}-\alpha\vec{K}_s|} \quad . \tag{74}$$

Matrix Elements

In this section we present the formulations for the matrix elements of the angular momentum and the current operator with the APW wavefunctions in Eq. (66).

Angular momentum matrix elements

It is very difficult to calculate the angular momentum matrix elements using the exact wavefunctions, Eq. (66) because the geometry involved in the integrals is complicated. Therefore we use a spherical approximation in which the unit cell is approximated by a sphere of the same volume (Wigner-Seitz sphere). The wavefunctions in the interstitial regions are approximated by the continuously extended spherical waves from inside the muffin-tin sphere. The angular momentum matrix elements are then written as

$$\int_{\substack{\text{W.S.}\\ \text{sphere}}} \varphi^*_{\vec{k},E}\, L_z\, \varphi_{\vec{k}'E'}\, d\vec{r}$$

$$= -i\sum_{\ell m}\sum_{\ell' m'} A^*_{\ell m} A'_{\ell' m'} \int_0^{r_{WS}} R_{\ell,E}(r) R_{\ell' E'}(r) r^2 dr \int Y^*_{\ell m}\, m'\, Y_{\ell' m'}\, d\Omega$$

$$= -i\sum_{\ell m} l_{\ell E E' m} A^*_{\ell m} A'_{\ell m} \tag{76}$$

where we used the orthogonality relations between the spherical Harmonics to obtain Eq. (76) from Eq. (75), and $I_{\ell EE'}$ in Eq. (76) is the radial integral

$$I_{\ell EE'} = \int_0^{r_{WS}} R_{\ell E}(r) R_{\ell E'}(r) r^2 dr \ . \tag{77}$$

Similarly we can show that

$$\int_{\substack{W.S.\\ \text{sphere}}} \varphi^*_{\vec{k}E} L_{\pm} \varphi_{\vec{k}'E'} d\vec{r} = \sum_{\ell m} I_{\ell EE'} \sqrt{(\ell \mp m')(\ell \mp m' + 1)}\ A^*_{\ell m} A'_{\ell m'}$$

$$\times \delta_{m,m' \pm 1} \tag{78}$$

where

$$L_{\pm} = L_x \pm i L_y \ .$$

Current matrix elements

We can calculate the current matrix elements exactly by using the wavefunctions in Eq. (66).

First of all, the matrix elements outside the muffin-tin sphere can be formulated as

$$\int_{\text{out}} \varphi^*_{\vec{k}E}(\vec{r}) [e^{i\vec{G}\cdot\vec{r}} \vec{\nabla}] \varphi_{\vec{k}'E'}(\vec{r})\, d\vec{r} \tag{79}$$

$$= \sum_{nn'} A^*_n A'_{n'} \int_{\text{out}} e^{-i(\vec{k}+\vec{K}_{n'})\cdot\vec{r}}\, e^{i\vec{G}\cdot\vec{r}} \vec{\nabla} e^{i(\vec{k}+\vec{K}_{n'})\cdot\vec{r}}\, d\vec{r} \tag{80}$$

$$= i \sum_{nn'} A_n^* A_{n'} (\vec{k}+\vec{K}_{n'}) \int_{out} e^{i(-\vec{K}_n + \vec{G} + \vec{K}_{n'}) \cdot \vec{r}} d\vec{r} \tag{81}$$

$$= i \sum_{nn'} A_n^* A_{n'} (\vec{k} + \vec{K}_{n'}) S (- \vec{K}_n + \vec{G} + \vec{K}_{n'}) \tag{82}$$

where S is the overlapping integral defined in Eq. (65).

The current matrix elements[28] for inside the muffin-tin sphere can be shown to be

$$\int_{in} \varphi^*_{\vec{k},E}(\vec{r}) [e^{i\vec{G}\cdot\vec{r}} \nabla_q] \varphi_{\vec{k}'E'}(\vec{r}) d\vec{r} \tag{83}$$

$$= 4\pi \sum_{KQ} i^K Y^*_{KQ}(\hat{G}) \sum_{\substack{\ell m \\ \ell' m'}} A^*_{\ell m} A'_{\ell' m'} \int d\Omega Y^*_{\ell m}(\hat{r}) Y_{KQ}(\hat{r})$$

$$\times \int dr\, r^2 j_K(Gr) R_{\ell E}(r) \{ \nabla_q R_{\ell' E'}(r) Y_{\ell' m'}(\hat{r}) \} \tag{84}$$

$$= 4\pi \sum_{KQ} i^K Y_{KQ}(\hat{G}) \sum_{\ell'} (-1)^{\ell'}$$

$$\times [\sqrt{\ell'} \sum_{\ell} \{ \int dr\, r^2 j_K(Gr) R_{\ell E}(r) (\frac{d}{dr} + \frac{\ell' + 1}{r}) R_{\ell' E'}(r) \}$$

$$\times \sum_m (-1)^m G^{\ell m}_{K-Q,\, \ell'-1 Q}, A^*_{\ell m} A'_{\ell' m'} \begin{pmatrix} \ell'-1 & 1 & \ell' \\ Q_1 & -q & -m' \end{pmatrix}$$

$$- (-1)^{\ell'} \sqrt{\ell' - 1} \sum_{\ell} \{ \int dr\, r^2 j_K(Gr) R_{\ell E}(r) (\frac{d}{dr} - \frac{\ell'}{r}) R_{\ell' E'}(r)$$

$$\times \sum_{m} (-1)^{m} G^{\ell m}_{K-Q,\,\ell'+1Q_1} A^{*}_{\ell m} A'_{\ell' m'} \begin{pmatrix} \ell'+1 & 1 & \ell' \\ Q_1 & -q & -m' \end{pmatrix}] \tag{85}$$

where $\begin{pmatrix} j_1 & j_2 & j_3 \\ m_1 & m_2 & m_3 \end{pmatrix}$ are the 3j symbols,[29] which gives us a selection rule, $m_1 + m_2 + m_3 = 0$, and $G^{\ell' m'}_{LM,\ell m}$ are the Gaunt's coefficients[29,30] defined by

$$G^{\ell' m'}_{LM,\ell m} = \int Y_{\ell' m'}(\hat{r})\, Y^{*}_{LM}(\hat{r})\, Y_{\ell m}(\hat{r})\, d\Omega\,, \tag{86}$$

$$= (-1)^{-m'} \left[\frac{(2\ell'+1)(2L+1)(2\ell+1)}{4\pi}\right]^{\frac{1}{2}} \begin{pmatrix} \ell' & L & \ell \\ -m & M & m \end{pmatrix} \begin{pmatrix} \ell' & L & \ell \\ 0 & 0 & 0 \end{pmatrix}. \tag{87}$$

The 3j symbols involved in Eq. (85) determine the selection rules Q_1 and m' in Eq. (85). In Eqs. (84) and (85), we used the plane wave expansion of Eq. (62) for $e^{-i\vec{G}\cdot\vec{r}}$, and following relations[28,31,32]

$$\nabla_q \{R(r)\, Y_{\ell m}(\hat{r})\} = \frac{1}{2} [\nabla^2, r_q] \{R(r) Y_{\ell m}(\hat{r})\} \tag{88}$$

$$= \frac{1}{2} \sum_{LM} \sqrt{(2\ell+1)(2L+1)} \begin{pmatrix} 1 & \ell & L \\ q & m & M \end{pmatrix} \begin{pmatrix} 1 & \ell & L \\ 0 & 0 & 0 \end{pmatrix} \nabla^2 \{rR(r)\, Y^{*}_{LM}(\hat{r})\}$$

$$- \frac{i}{2} \left\{\sqrt{\frac{4\pi}{3}}\, r\, Y_{1q}(\hat{r})\right\} \nabla^2 R(r)\, Y_{\ell m}(\hat{r})$$

$$= -\sqrt{\ell+1} \left(\frac{d}{dr} - \frac{\ell}{r}\right) R(r) \sum_{M} (-1)^{q+m+\ell} Y_{\ell+1,M}(\hat{r}) \begin{pmatrix} \ell-1 & 1 & \ell \\ M & -q & -m \end{pmatrix}$$

$$+ \sqrt{\ell} \left(\frac{d}{dr} + \frac{l+1}{r}\right) R(r) \sum_{M} (-q)^{q+m+\ell} Y_{\ell-1,M}(\hat{r}) \begin{pmatrix} \ell-1 & 1 & \ell \\ M & -q & -m \end{pmatrix} \tag{89}$$

where the tensors ∇_q, $\hat{r}_q$ of rank 1 used above are defined by

$$\nabla_{\pm 1} = \mp \frac{1}{\sqrt{2}} \left(\frac{\partial}{\partial x} \pm i \frac{\partial}{\partial y} \right)$$

$$\nabla_0 = \frac{\partial}{\partial z} \tag{90}$$

and

$$r_{\pm 1} = \mp \frac{1}{\sqrt{2}} (x \pm iy)$$

$$r_0 = z$$

or

$$r_q = \sqrt{\frac{4\pi}{3}}\, r\, Y_{1q}(\hat{r}) \tag{91}$$

k-Space integrals

The k-space integrals[33,34,35] which need to be calculated in the present study are the density of states function Eq. (35) and the neutron magnetic form factor Eq. (49). These functions can be written again in summation forms as

$$D(E) = 2 \sum_{ni} \frac{\Delta S_n(E, \bar{k}_i)}{|\nabla_k E_n(\bar{k})|_{\bar{k}=\bar{k}_i}}, \tag{35}$$

and

$$\chi = \sum_{nn'k} \frac{f_{nk}(1 - f_{n'k})}{E_{n'k} - E_{nk}} |m.e.|^2 \quad . \tag{49'}$$

In order to calculate these functions, we, first of all, break the Brillouin zone into small microzones (tetrahedrons in the present case) and assume that energy eigenvalues inside each tetrahedron can be determined in a certain fashion in terms of the four corner energies ($E_4 \leq E_3 \leq E_2 \leq E_1$). A simple approach for this is the linear interpolation, in which the energy eigenvalues are determined by

$$E(\vec{k}) = E(\vec{k}_4) + \vec{b} \cdot (\vec{k} - \vec{k}_4) \tag{92}$$

where

$$\vec{b} = \sum_{i=1}^{3} [E(\vec{k}_i) - E(\vec{k}_4)] \vec{R}_i \tag{93}$$

and

$$\vec{R}_i \cdot \vec{k}_j' = \delta_{ij} \ , \tag{94}$$

with

$$\vec{k}_j' = \vec{k}_j - \vec{k}_4 \ . \tag{95}$$

The R_i's can then be found from

$$\vec{R}_i = \frac{\vec{k}_j' \times \vec{k}_\ell'}{V} \ , \quad (i\ j\ \ell \text{ are cyclic}) \tag{96}$$

where $V = \vec{k}_1' \cdot (\vec{k}_2' \times \vec{k}_3')$ = 6x volume of the tetrahedron. The advantage for this linear energy interpolation is that the surface of a constant energy becomes a simple plane inside the tetrahedron. This allows us to obtain analytic expressions for the surface area and the occupied volume inside each tetrahedron. From considerations of the general geometric properties of the cross-sectional area of a plane intersecting the i^{th} tetrahedron, the analytic expression for the area can be shown to be[34,35]

$$\frac{\Delta S(E)}{|\vec{b}|} = \begin{cases} f_0 & E_4 \le E \le E_3 \\ f_0 - f_1 & E_3 \le E \le E_2 \\ f_2 & E_2 \le E \le E_1 \\ 0 & E \le E_4 \text{ or } E_1 \le E \end{cases} \tag{97}$$

where

$$f_0 = \frac{V}{2} \frac{(E - E_4)^2}{(E_3 - E_4)(E_2 - E_4)(E_1 - E_4)} ,$$

$$f_1 = \frac{V}{2} \frac{(E - E_3)^2}{(E_3 - E_4)(E_2 - E_3)(E_1 - E_3)} ,$$

$$f_2 = \frac{V}{2} \frac{(E - E_1)^2}{(E_1 - E_4)(E_1 - E_3)(E_i - E_2)} . \tag{98}$$

As is clear from these analytic expressions, energy gradients do not occur explicitly and the density of state functions can be calculated accurately if the Brillouin zone is divided into a large number of small enough tetrahedrons.

The neutron magnetic form factor can be calculated similarly as was done for the density of states. The fractional volume of a tetrahedron that contributes to the form factor, that is, $f_{nk}(1 - f_{nk}) = 1$, is determined by intersection of constant energy surface corresponding to E_{nk}. (Note that $E_{n'k}$ should be always less than E_4.) This fractional volume can be shown to be either a tetrahedron or a sum of three tetrahedrons. Thus after taking care of the Fermi factors, a volume integration over this fractional volume with a linearized energy denominator is left to be performed assuming the matrix elements are constant inside the tetrahedron. This can be done easily to give[36]

$$\sum_k \frac{f_{nk}(1 - f_{nk})}{E_{n'k} - E_{nk}} |\text{m.e.}|^2$$

$$\simeq \frac{\Omega}{(2\pi)^3} \sum_{\substack{\text{occupied} \\ \text{tetras}}} |\text{m.e.}|^2 \int_{\substack{\text{each} \\ \text{tetra}}} \frac{d\vec{k}}{E_{n'}(\vec{k}) - E_n(\vec{k})}$$

$$= \frac{\Omega}{(2\pi)^3} \sum_{\substack{\text{occupied} \\ \text{tetras}}} |\text{m.e.}|^2 \left[\frac{V_1^2}{D_1} \ell n \left|\frac{V_1}{V_4}\right| + \frac{V_2^2}{D_2} \ell n \left|\frac{V_2}{V_4}\right|\right.$$

$$\left. + \frac{V_3^2}{D_3} \ell n \left|\frac{V_3}{V_4}\right|\right] \tag{99}$$

where

$$V_i = E_{n'}(\vec{k}_i) - E_n(\vec{k}_i) \ , \tag{100}$$

and

$$D_i = \prod_{\substack{j=1 \\ j \neq i}}^{4} (V_i - V_j) \ . \tag{101}$$

For the case when some of V_i's are zero or equal, one must take the limit of Eq. (99). Thus again we see that the neutron magnetic form factor can be calculated by this tetrahedron method assuming the matrix elements are uniform inside each tetrahedron. This is a good approximation if the tetrahedrons are chosen to be small enough.

CHAPTER IV. RESULTS AND DISCUSSION

Energy Band and Wavefunction

Chromium has a body-centered cubic (BCC) symmetry with a lattice constant 5.451 au. Figure 1 shows the Brillouin zone of the BCC lattice, and its 1/48th irreducible zone is shown by the shaded region in this figure. We employed the APW method for the first principle calculation of energy bands and wavefunctions of paramagnetic chromium. In this calculation, we used a so-called compressed mesh, which is defined by compressing the mesh points inside the 1/48th zone towards the center of it. For example, the compressed π/Na mesh has (k_x,k_y,k_z) coordinates determined by

$$\begin{aligned} k_x &= M_x - \Delta_1 x|M_x - N|x(M_x - N), \\ k_y &= M_y - \Delta_2 x|M_y - N/2|x(M_y - N/2), \\ k_z &= M_z - \Delta_3 x|M_z - N/2|x(M_z - N/2) - \Delta_4, \end{aligned} \tag{102}$$

where M_x, M_y and M_z run from 0 to 2N, N and N respectively, and Δ's are small numbers. The reason for using this compressed mesh is because when there is a degeneracy of energy eigenvalue, the wavefunction character for a particular band may change abruptly, and thus the matrix elements with these wavefunctions can not be interpolated smoothly along with other matrix elements calculated with nearby nondegenerate states. The mesh points determined by Eq. (102) are away from the high symmetry planes. Thus we expect the eigenvalues calculated with this mesh to be nondegenerate except the accidental ones because eigenvalue degeneracy occurs on the high symmetry planes. We used a $\pi/6a$ compressed mesh

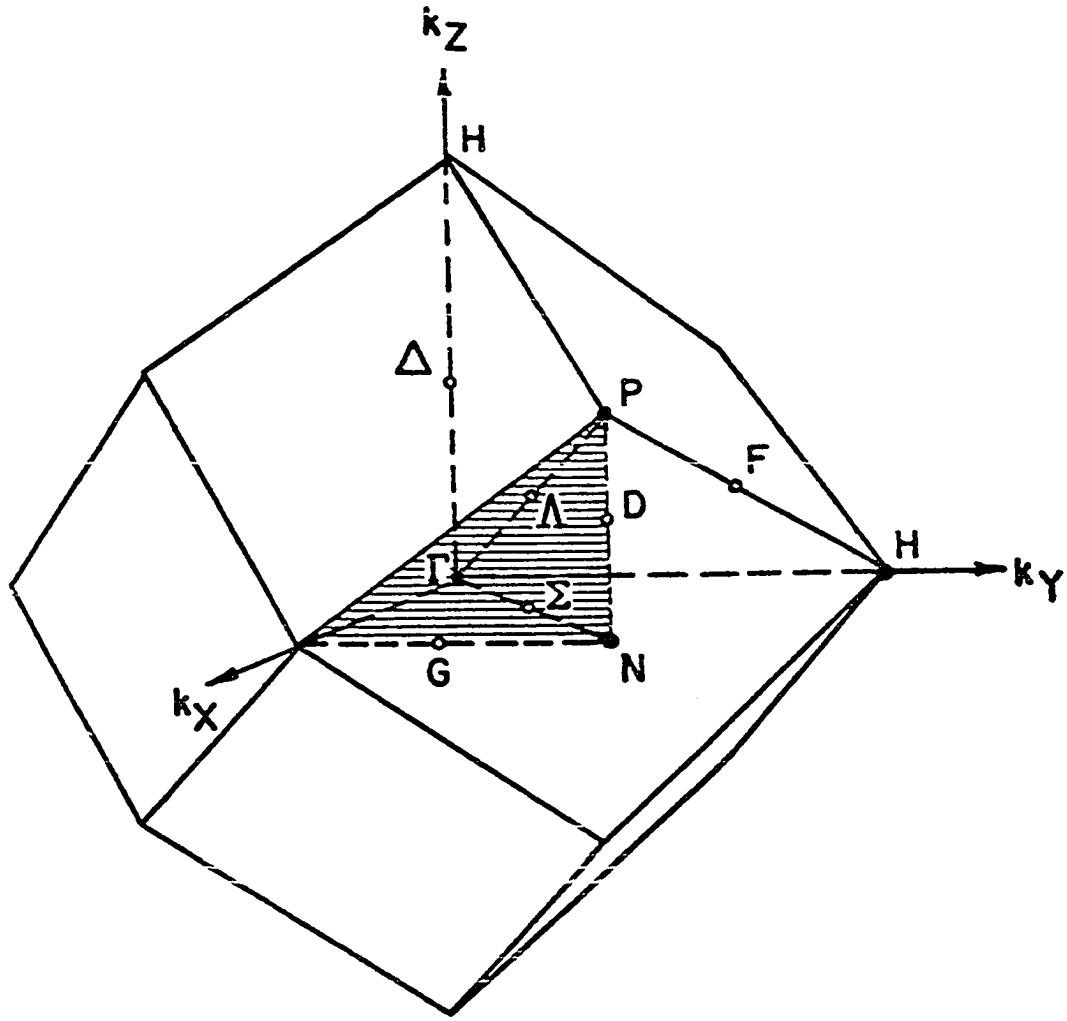

Fig. 1. Brillouin zone of a body center cubic lattice. Shaded region represents a 1/48th irreducible zone.

(total 140 mesh points inside the 1/48th Brillouin zone) with Δ_1=0.003 and $\Delta_2=\Delta_3=\Delta_4$=0.01 in this study. The mesh points on the first layer of $\pi/6a$ mesh are shown in Fig. 2. The energy eigenvalues calculated with this compressed mesh usually give splittings of degeneracies of a few tenth of a milli-Rydberg. In Fig. 3, we plot the calculated energy bands along the high symmetry directions in the compressed mesh. The energy scale in this plot was not large enough to show the splittings of degenerate bands. Figure 4 shows the percentage of ℓ characters of the wavefunctions for each band, which were calculated by using the Wigner-Seitz approximation. It is interesting to see that the bands 3, 4 and 5 which cut the Fermi surface are mostly d-like except near N. Since the form factor depends mostly on bands near the Fermi surface, this seems to be a plausible reason why the 3d atomic form factor yields good agreement with experiments.

The calculated energy bands were least squares Fourier fitted with 60 symmetrized plane waves, and we used the Fourier coefficients to generate the eigenvalues for any arbitrary mesh points. The r.m.s. errors of the chromium energy band fitting are a few milli-Rydbergs. This Fourier fit needs to be used carefully when there is a band crossing. This is because each Fourier fitted band with a finite number of basis functions can not reproduce the sharp kinks which result from band crossings. They smooth out the sharp kinks, and instead small inevitable gaps appear at the places where there should be band crossings. This point was not, however, important in the form factor calculations, but its effect was observed in the Fermi surface plot.

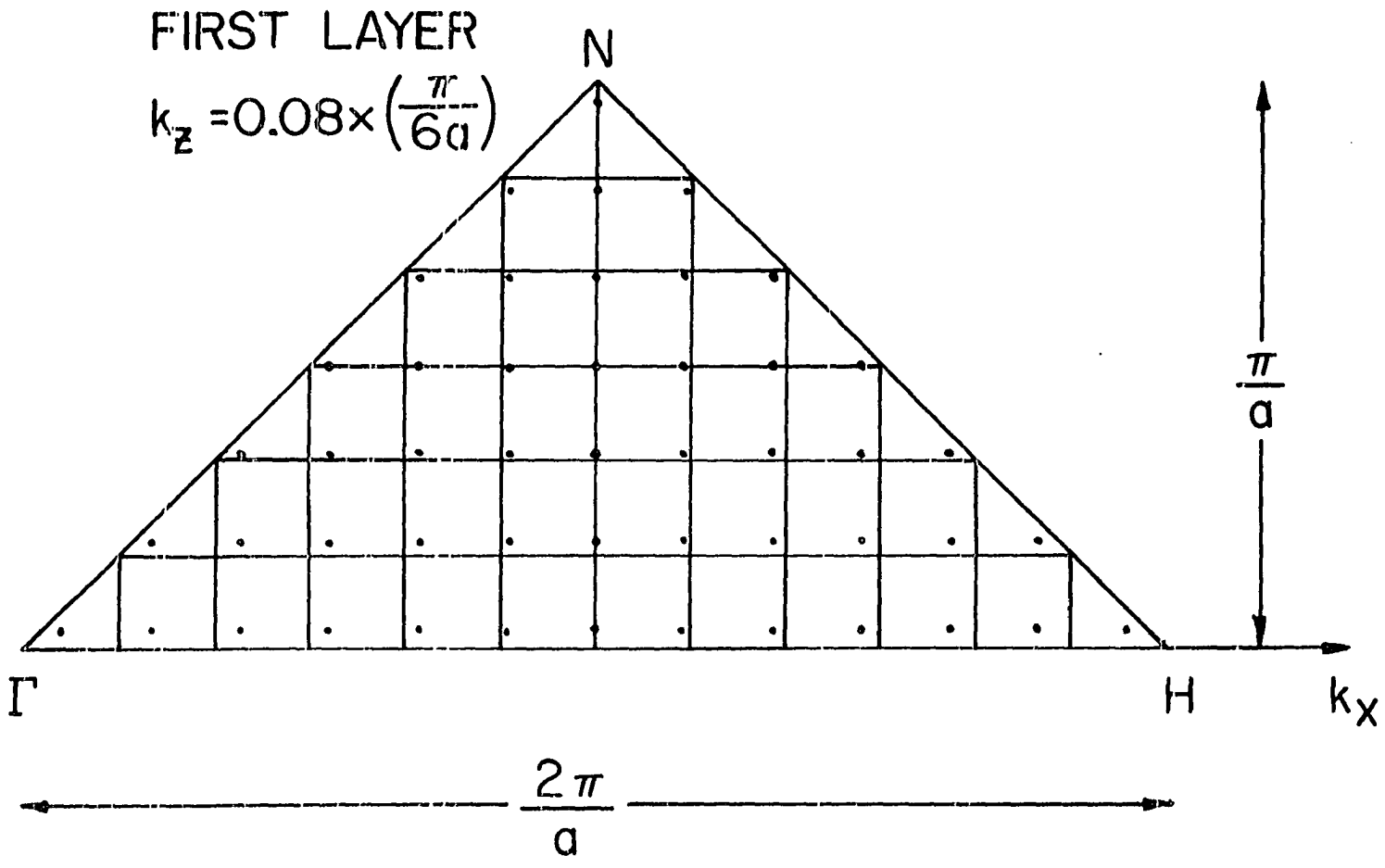

Fig. 2. Mesh points on the first layer of a π/6a compressed mesh.

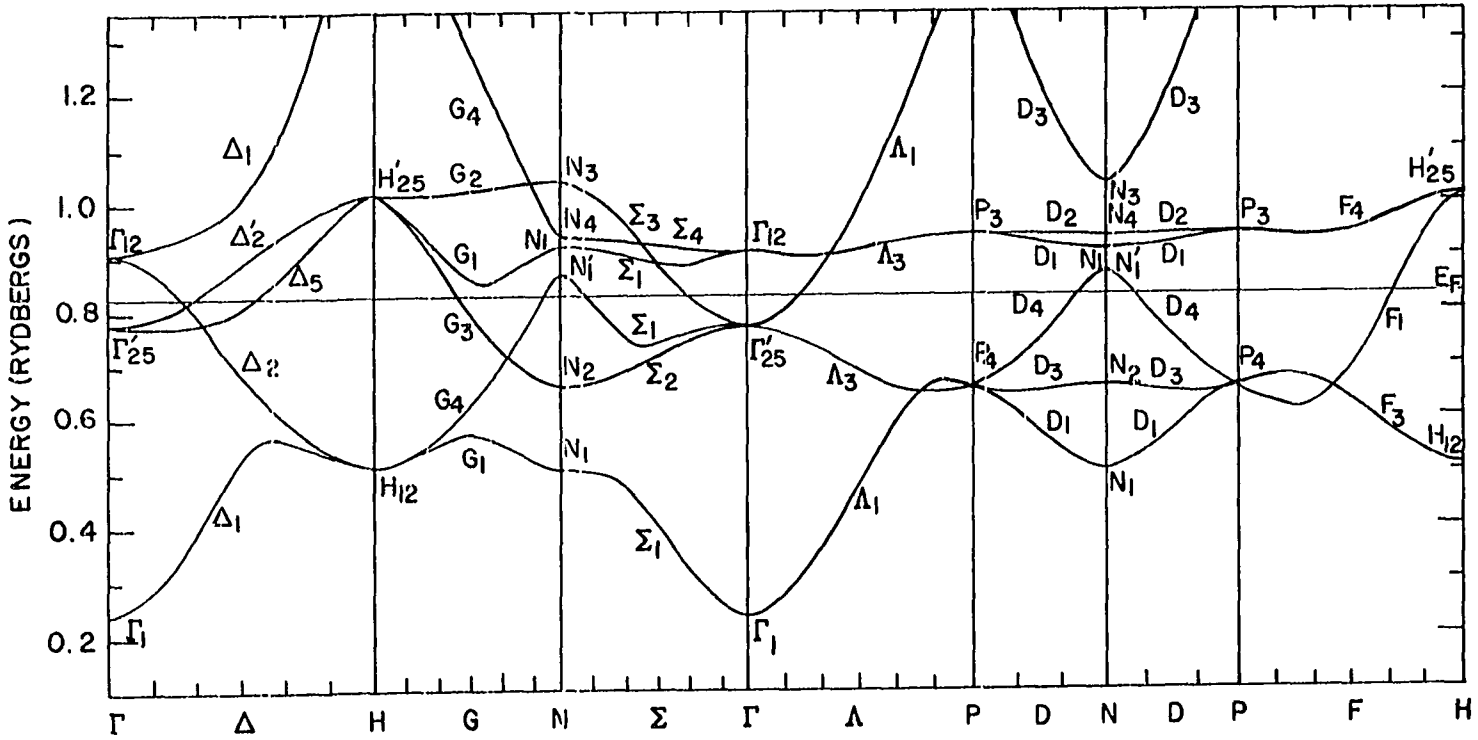

Fig. 3. Energy bands of Cr along high symmetry directions.

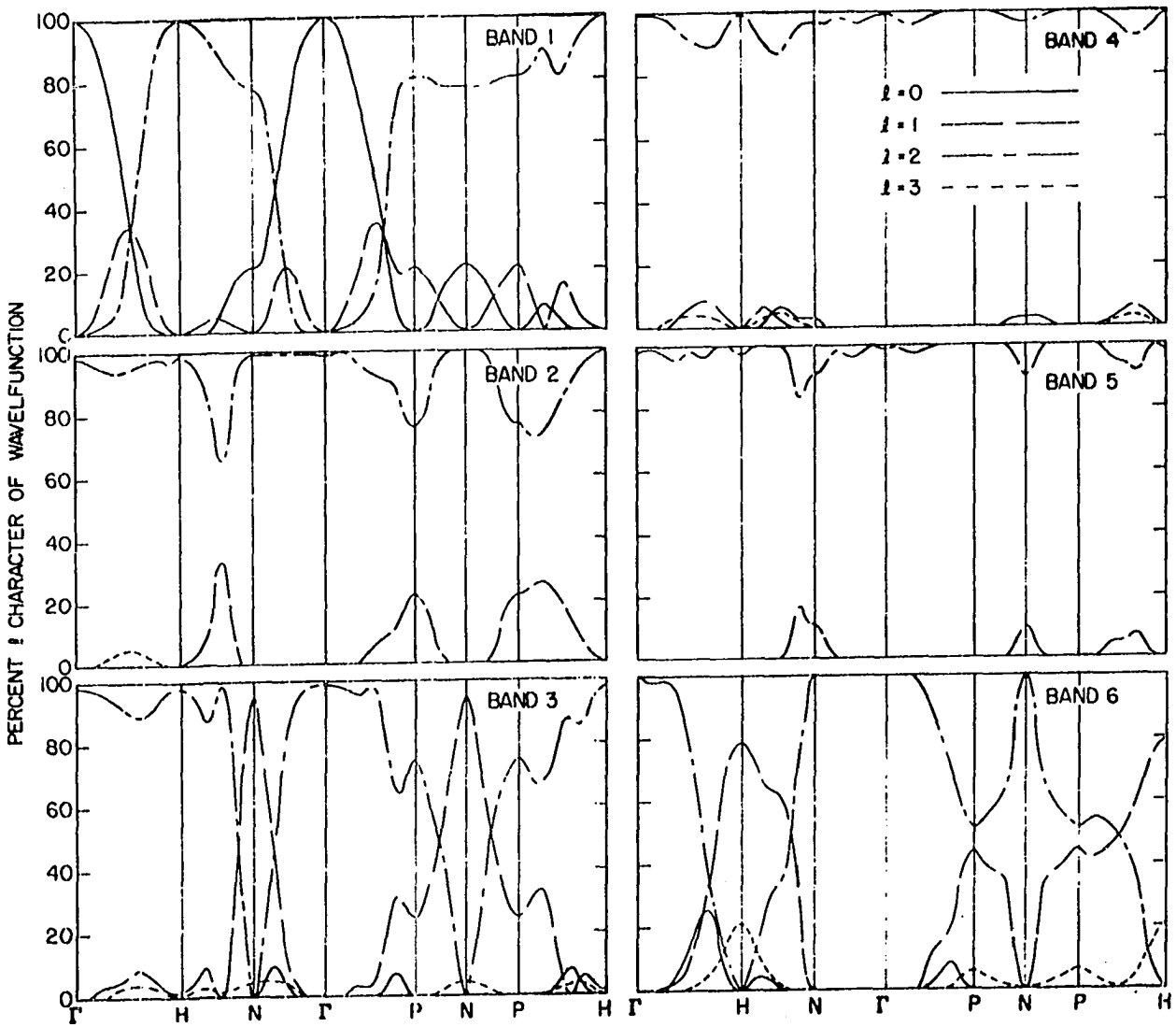

Fig. 4. Percentage ℓ character of Cr wavefunctions along high symmetry directions.

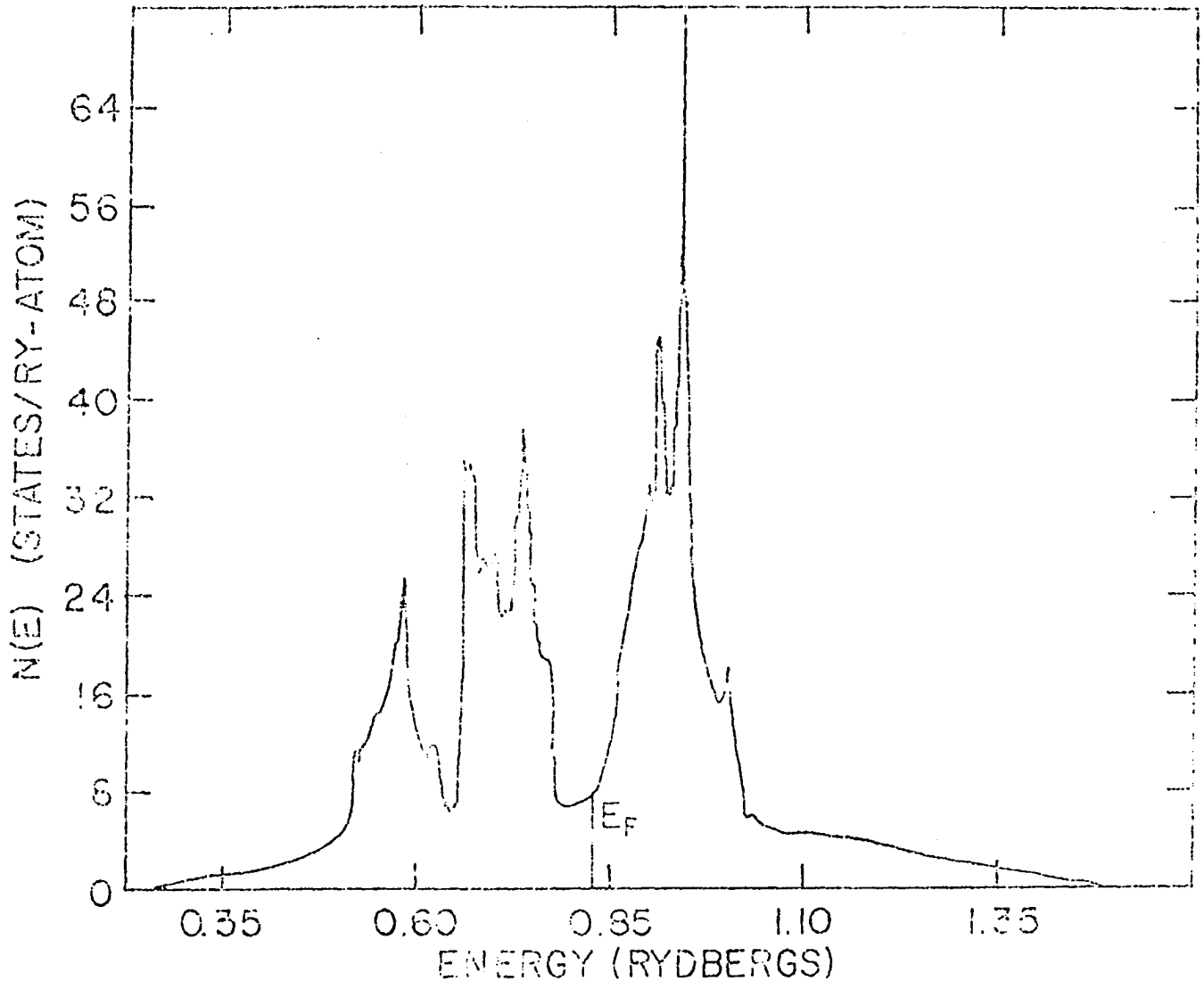

Fig. 5. Density of states of Cr. Fermi energy (E_F) is 0.829 Ry.

The density of states were calculated by using the tetrahedron method. The energies at the four corners of the tetrahedron were calculated with the Fourier fit coefficients. The resulting curve is shown in Fig. 5. each of the five peaks at E=0.569, 0.653, 0.727, 0.911, and 0.939 Ry in the density of states was found to be arising from bands 1 to 5 respectively. The Fermi energy occurs at 0.829 Ry, and the density of states at this value of energy is found to be 7.90 states/Ry-atoms.

Spin Form Factor

With the density of states at the Fermi energy (7.90 states/Ry-atoms) the Pauli spin susceptibility,

$$\chi_{Pauli} = \mu_B^2 D(E_F) \tag{34}$$

has the value 18.79×10^{-6} emu/mole. This is smaller than the experimental value[5] by a factor of about 3. Thus we need a large enhancement for the spin form factor. For the calculation of the induced spin form factor for $\vec{G}$ other than 0, we at first calculated the crystal charge density at the Fermi energy Eq. (37) in the following way:
We use the tetrahedron method to find the cross sections in the tetrahedrons which are cut by the Fermi surface so that we can approximate the Fermi surface by these cross sectional areas. The charge densities on these cross sectional areas are then calculated by using the wavefunctions at the center of mass of these cross sections. These charge densities on the cross sectional areas are finally used to calculate the averaged crystal charge density at $E=E_F$.

There were 202 tetrahedrons for the $\pi/8a$ mesh which cut the Fermi

surface. As mentioned before, the cross section, i.e. the constant energy surface at $E=E_F$, becomes a plane if energy is assumed to have a linear dependence on $\vec{k}$ inside each tetrahedron. This simplifies the calculation of the cross sectional areas and the $\vec{\nabla}_k$ E's in each tetrahedron. The numerical results were used to estimate the weights $(\frac{\Delta S}{|\nabla E|})$ for the 202 crystal charge densities at $E=E_F$. Using these 202 crystal charge densities, the averaged crystal charge density at $E=E_F$ (both inside and outside of the muffin-tin sphere) was calculated as described in Eqs. (68) and (70). This was used to calculate the final spin form factor following the recipe in the previous chapter. The numerical results of the induced spin form factor are shown in Table 1, and its plot (which is normalized to 1 at $\vec{G}=0$) in Fig. 6. We also plotted the 3d free ion spin form factor of Freeman and Watson[2] in Fig. 6.

Our calculated induced moment spin form factor appears to be more contracted than the 3d free ion spin form factor. In order to understand this fact, we calculated the 3d atomic crystal charge densities by performing the Löwdin alpha sum of the Hartree-Fock-Slater atomic 3d charge densities. These are shown in Fig. 7 together with the radial part of the crystal wavefunction at $E=E_F$, $C_L(r)$ in Eq. (72). This shows that the crystal charge density is more extended than the 3d atomic crystal charge density. This seems to be the reason why our calculated induced spin form factor is more contracted than the 3d only free ion spin form factor. Figure 7 also shows the aspherical contribution of the crystal charge density at $E=E_F$, $C_4(r)$ in Eq. (72), which gave rise to the anisotropies in our induced spin form factor.

Table I. Calculated values of the induced Pauli type spin (χ_s) and Van Vleck type orbital (χ_{vv}) form factors of Cr. Normalized values of χ_s and χ_{vv} are shown in brackets. Experimental results are from Stassis et al.[4] which are normalized to 163×10^{-6} emu/mole to compare with our values.

$\vec{G}$	Sin θ/λ	χ_s ($\times 10^{-6}$ emu/mole)	χ_{vv} ($\times 10^{-6}$ emu/mole)	χ_{tot} ($3.3\chi_s + .78\chi_{vv}$) ($\times 10^{-6}$ emu/mole)	Experiments[4] ($\times 10^{-6}$ emu/mole)
0 0 0	0.000	18.79 (1.000)	130.00 (1.000)	163.40	163.00
1 1 0	0.245	7.52 (0.400)	87.36 (0.672)	92.93	92.64
2 0 0	0.347	3.68 (0.196)	60.32 (0.464)	59.22	60.61
2 1 1	0.425	2.84 (0.151)	-----	-----	48.41
2 2 0	0.490	1.88 (0.100)	-----	-----	36.04
3 1 0	0.548	0.66 (0.035)	-----	-----	-----
2 2 2	0.600	1.20 (0.064)	-----	-----	-----
3 2 1	0.649	0.56 (0.030)	-----	-----	19.82
4 0 0	0.693	-0.53 (-.028)	16.43 (0.126)	10.80	-----
3 3 0	0.735	0.23 (0.012)	14.12 (0.109)	11.77	11.63
4 1 1	0.735	-0.28 (-.015)	-----	-----	6.80
4 2 0	0.775	-0.15 (-.008)	-----	-----	-----

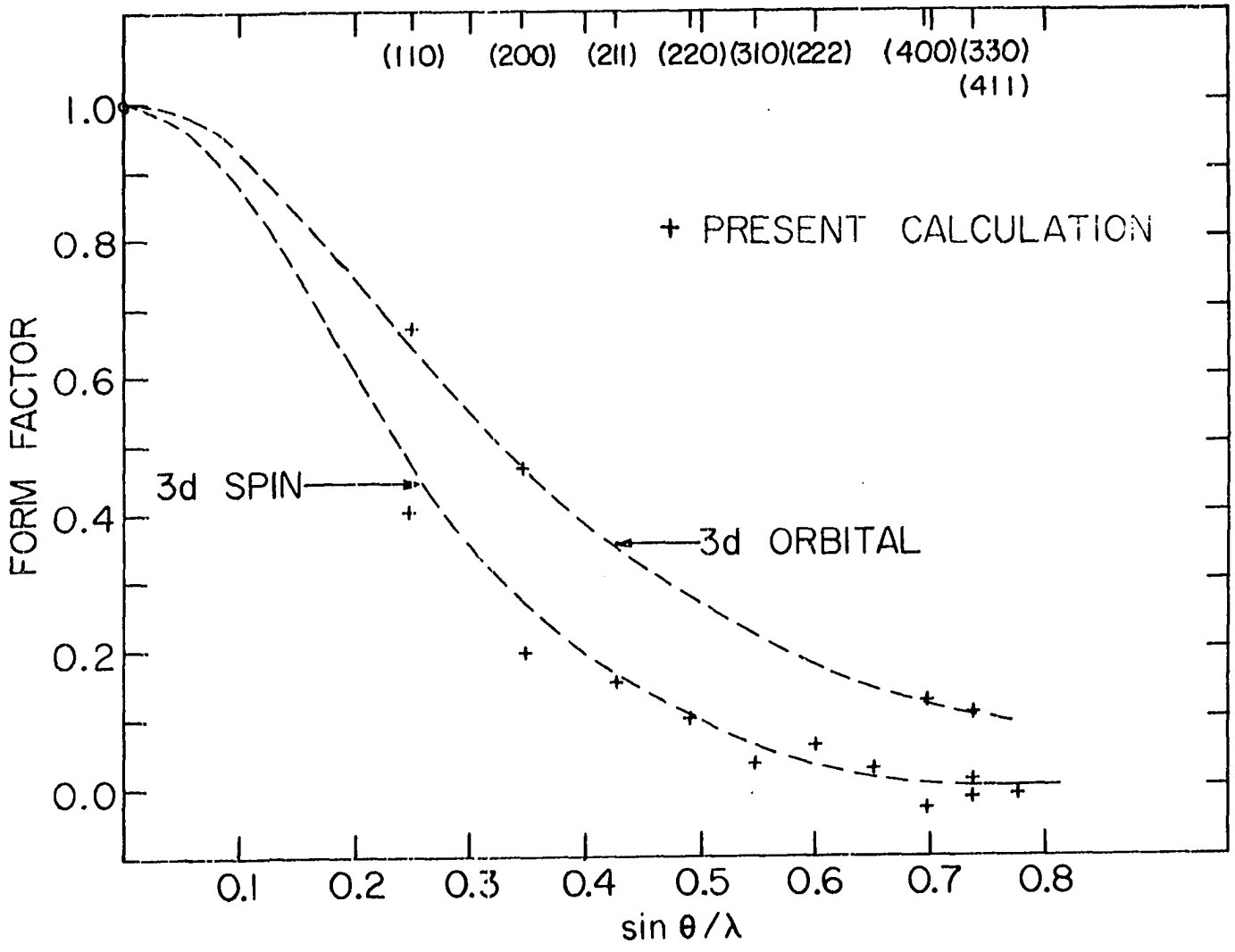

Fig. 6. Normalized spin and orbital magnetic form factors of Cr to compare with 3d free ion form factors of Freeman and Watson.

Fig. 7. Crystal charge density of Cr at $E=E_F$ and 3d atomic crystal charge density of Cr which were calculated by the Löwdin α sum of Hartree-Fock-Slater 3d charge density.

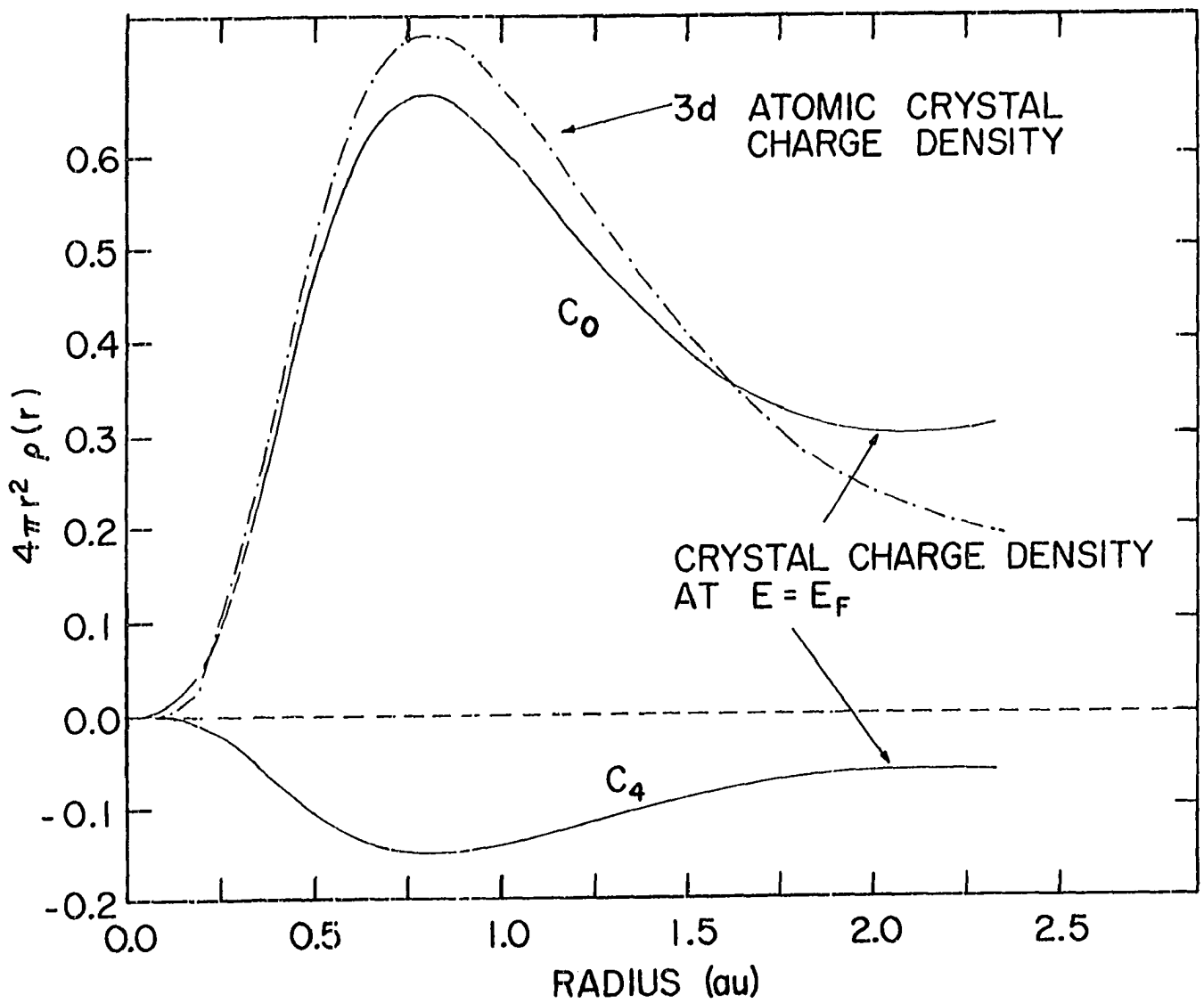
3d ATOMIC CRYSTAL CHARGE DENSITY
C_0
CRYSTAL CHARGE DENSITY AT $E = E_F$
C_4
$4\pi r^2 \rho(r)$
0.6
0.5
0.4
0.3
0.2
0.1
0.0
-0.1
-0.2
0.0
0.5
1.0
1.5
2.0
2.5
RADIUS (au)

Orbital Form Factor

In order to obtain the induced Van Vleck type orbital form factor, namely, the second term in Eq. (49),

$$\chi_{vv}(G,0) = -\frac{ie^2}{m^2c^2G}\sum_{nkn'}\frac{f_{nk}-f_{n'k}}{E_{n'k}-E_{nk}}\langle n\vec{k}|p_x e^{-iGy}|n'\vec{k}\rangle\langle n'\vec{k}|L_z|n\vec{k}\rangle \qquad (103)$$

we had to calculate the matrix elements of the angular momentum operator (L_z) and the current operator ($p_x e^{-iGy}$), and perform the summation of its products over the whole Brillouin zone. The number of transitions between the occupied bands and the unoccupied bands we considered here was 13, namely, (1-3), (1-4), (1-5), (1-6), (2-3), (2-4), (2-5), (2-6), (3-4), (3-5), (3-6), (4-5), and (4-6) band pairs. Here we did not include the (5-6) transition because the phase space volume involved in this transition is too small.

We calculated the angular momentum and current matrix elements for the 13 band pairs for each of the 140 $\vec{k}$ values. The Wigner-Seitz approximation was made to calculate the angular momentum operator matrix elements, and rigorous calculation by using the Bloch wavefunctions was made for the current operator matrix elements following the formula Eq. (85). Since we calculated the wavefunctions only inside the 1/48th of Brillouin zone, we had to apply group theory to the wavefunctions inside the 1/48th zone in order to obtain the wavefunctions for other parts of the Brillouin zone. For a fixed $\vec{k}$, angular momentum operator has only three independent matrix elements in the entire Brillouin zone. Therefore we only needed to calculate the matrix elements (L_x, L_y, L_z) inside the 1/48th of Brillouin zone, and obtain the others from them

by using rotational arguments. Whereas we had to calculate the current matrix elements in the 1/8th of the Brillouin zone for $\vec{G}=(G_x,0,0)$, and in the 1/4th of the zone for $\vec{G}=(G_x,G_y,0)$ in order to obtain the current matrix elements in the entire Brillouin zone. Again we used group theoretical arguments, for example, $\langle n,(k_x,k_y,k_z)|p_x e^{-iGy}|n',(k_x,k_y,k_z)\rangle = -\langle n,(-k_x,k_y,k_z)|p_x e^{-iGy}|n',(-k_x,k_y,k_z)\rangle$ to obtain the rest of the current matrix elements.

Finally, we are in a position to calculate the induced orbital form factor by performing the summations of the products of angular momentum and current matrix elements over the whole Brillouin zone via the tetrahedron method.[36,37] The products of the matrix elements are assumed to be constant throughout each small tetrahedron, and were approximated by averaging the values at four corners of the tetrahedron. The Van Vleck susceptibility at $\vec{G}=0$ was found to be 130.0×10^{-6} emu/mole, which is quite large compared with the experimental value.[4,5] The x-ray photoemission measurement of Ley et al.[38] showed a valence band width of 0.140 Ry, whereas the corresponding d band width of our band (with $\alpha=1$ exchange potential) is 0.121 Ry. These narrow bands would cause the orbital contribution to be somewhat large because of the smaller energy denominator in Eq. (103). However, we do not expect the shape of the orbital form factor to change appreciably.

It takes us three to four hours with the ISU computer (IBM 360/65) to compute the current matrix elements for one $\vec{G}$ value. Thus for financial reasons, we had to terminate the calculation after we obtained four reflections. We have not attempted to calculated the current matrix

elements for arbitrary $\vec{G}=(G_x,G_y,G_z)$ because it is very complicated and would take a much longer time to compute. The numerical results of the induced Van Vleck type orbital form factor are shown in Table 1, and its plot (which is normalized to 1 at $\vec{G}=0$) in Fig. 6 together with the spin form factor. The last two reflections, (4,0,0) and (3,3,0) were calculated to see if there is anisotropy in the orbital form factor. But no anisotropy is apparent from the result. Surprisingly enough, the calculated points fall right on the 3d free ion orbital form factor. It seems that, when we perform the integrals of the quantity which involves the crystal wavefunctions over the whole Brillouin zone, the averaged behavior of the crystal wavefunctions in the entire Brillouin zone resembles the 3d free ion wavefunction.

Discussion and Summary

In order to compare our calculated induced form factor with the neutron diffraction experimental results[4], we took the following facts into consideration: (1) the calculated induced spin form factor should be enhanced due to the exchange interaction, and (2) the diamagnetic contributions from the Landau terms, the core contributions, and the surface terms should be included in the orbital form factor.

As the exchange interaction is turned on, the compensated spin up and down electrons sense the effective field which is set up by the uncompensated spin up electrons. This effective field causes a further band splitting and increases the number of uncompensated spin up

electrons. Such exchange enhancement can be accounted[39,40] roughly by enhancing the charge densities at $E = E_F$ in Eq. (37) as

$$\rho(r) = \Lambda \mu_B^2 \sum_{\substack{nk \\ E=E_F}} \frac{\Delta S_n(\vec{k})}{|\nabla_k E_n(k)|} [1 + I(\vec{k})] \mid \varphi_{nk}(r) \mid^2, \qquad (104)$$

where $I(\vec{k})$ is the enhancement factor which is assumed to be small, and Λ is a normalization factor. We tried to calculate the spin form factor of Eq. (36) by enhancing the d components of the charge densities by 10%, i.e. by using the enhanced charge density of Eq. (104) with $I(\vec{k})$=0.1x(% of d electron charge density at $\vec{k}$). The shape of this enhanced spin form factor showed no appreciable change from the unenhanced one. Therefore we assumed the enhanced spin form factor has the same $\vec{Q}$ dependence as the unenhanced spin form factor. Next, we assumed the overall shape of the diamagnetic contributions and the surface terms in the orbital form factor is proportional to the Van Vleck type orbital form factor. Hence, we approximated the induced magnetic form factor from our calculated Pauli type spin (χ_s) and the Van Vleck type orbital (χ_{vv}) form factors in the following way:

$$\chi(G,0) = (1 + e)\, \chi_s(G,0) + (1 - d)\, \chi_{vv}(G,0) . \qquad (105)$$

Comparision of $\chi(G,0)$ with the experimental results of Stassis et al.[4] shows that there should be about a 330% (i.e. e=2.3) enhancement for the spin form factor, and the diamagnetic contributions

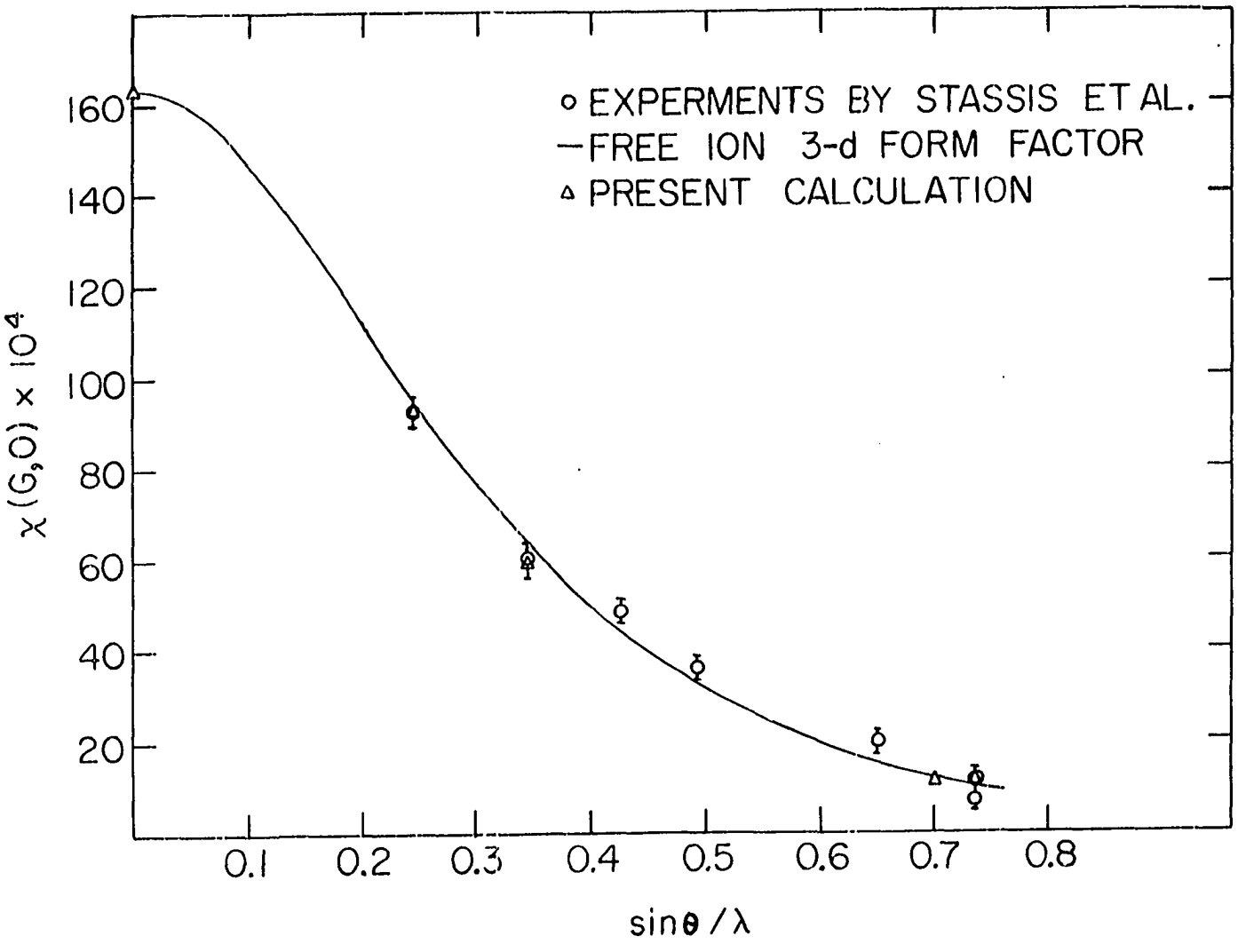

Fig. 8. Total adjusted induced magnetic form factor of Cr with the neutron diffraction experimental results and free ion 3d form factor of Cr.

should be about 22% of the Van Vleck type orbital form factor. This adjusted total induced magnetic form factor of Cr is shown in Table 1, and its plot in Fig. 8 together with the neutron diffraction results.[4] The 3d free ion form factor which consists of a 60% orbital and a 40% spin contributions is also shown in Fig. 8. The agreement between our calculated induced magnetic form factor and the experimental results[4] is extremely good. This analysis gives a spin susceptibility of 62×10^{-6} emu/mole and an orbital susceptibility of 101×10^{-6} emu/mole, which yields a gyromagnetic ratio of 1.23. This is a correct prediction of the gyromagnetic ratio of Cr, whose value was obtained experimentally to be 1.21 ± 0.07 by the Einstein-de Haas method.[5]

We formulated expressions for the induced magnetic form factor from first principles by using linear response theory, and applied it to metallic Cr to perform the numerical calculations of the induced Pauli type spin and the Van Vleck type orbital form factor. The required energy bands and Bloch wavefunctions were obtained from the APW method on a compressed $\pi/6a$ mesh. The calculated Van Vleck type orbital form factor was found to be isotropic, and is very similar to that of the 3d free ion form factor even though there are large differences in the radial functions for fifferent energies as shown in Fig. 9. The calculated total paramagnetic form factor of Cr shows good agreement with the neutron diffraction results of Stassis et al.[4]

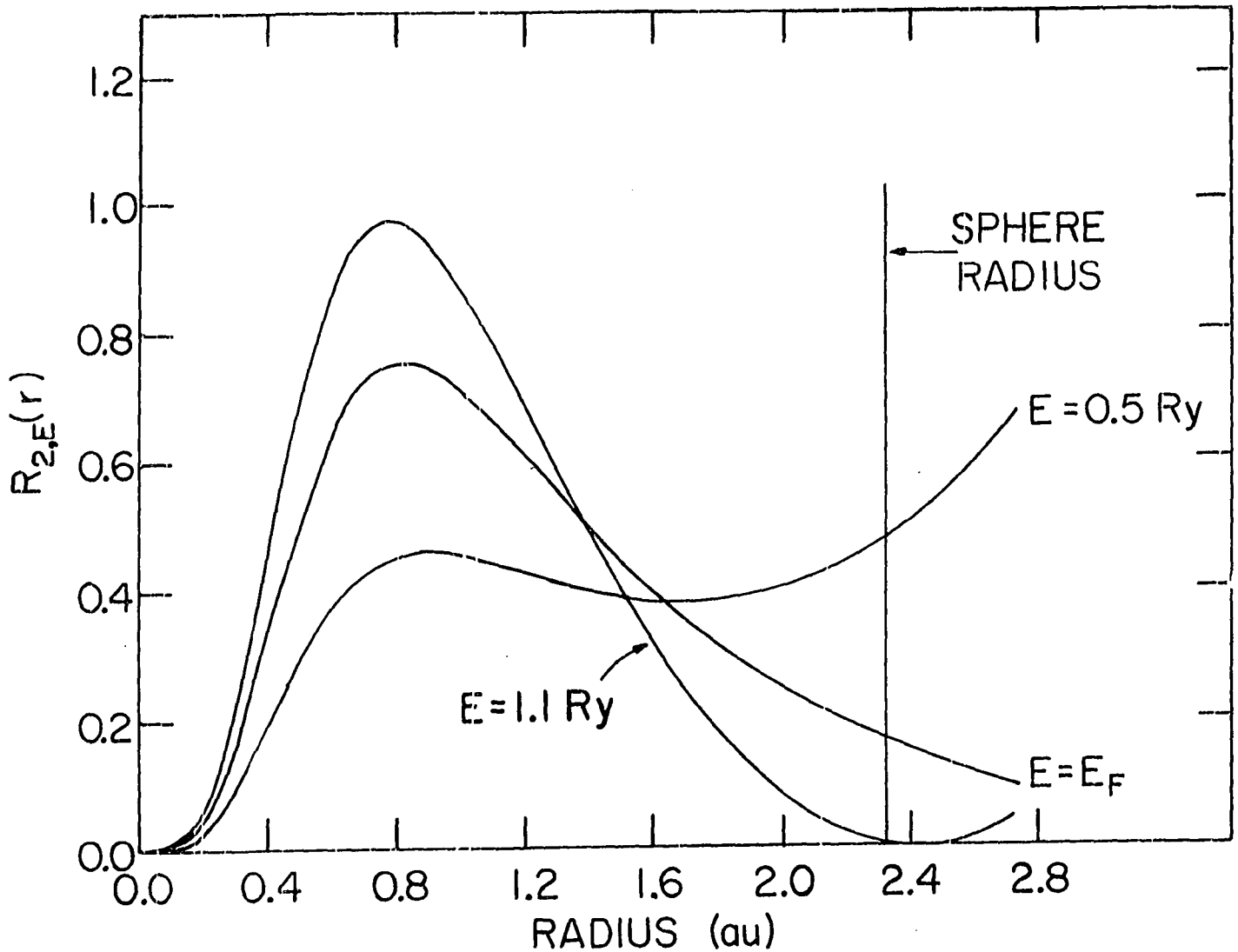

Fig. 9. Chromium 3d radial functions for energies below, at, and above E_F.

when we considered the diamagnetic contributions in the orbital form factor and an exchange enhancement of 3.3 in the spin form factor. This analysis shows that the spin susceptibility is 62×10^{-6} emu/mole and the orbital susceptibility 101×10^{-6} emu/mole, which predicts a correct gyromagnetic ratio of 1.23 compared with the Einstein-de Haas experimental value.[5]

BIBLIOGRAPHY

1. R. M. Moon, W. C. Koehler, and A. L. Trego, J. Appl. Phys. 37, 1036 (1966).

2. A. J. Freeman and R. E. Watson, Acta Cryst. 14, 231 (1961).

3. S. Asano and J. Yamashita, J. Phys. Soc. Japan 23, 714 (1967).

4. C. Stassis, G. R. Kline, and S. K. Sinha, Phys. Rev. Letters 31, 1498 (1973), and Phys. Rev. B (to be published).

5. R. Huguenin, G. P. Pells, and D. N. Baldock, J. Phys. F: Metal Phys. 1, 281 (1971).

6a. J. M. Ziman, Principles of the Theory of Solids (Cambridge University Press, London, 1969).

6b. J. H. Van Vleck, The Theory of Electric and Magnetic Susceptibilities (Oxford University Press, London, 1932).

7. R. Kubo and Y. Obata, J. Phys. Soc. Japan 11, 547 (1956).

8. L. E. Orgel, J. Phys. Chem. Solids 21, 123 (1961).

9. W. M. Lomer, Proc. Phys. Soc. (London) 82, 156 (1963).

10. L. Landau, Z. Physik 64, 629 (1930).

11. R. E. Peierls, Z. Physik 80, 763 (1933).

12. O. Halpern and M. H. Johnson, Phys. Rev. 55, 898 (1939).

13. M. Blume, Phys. Rev. 124, 96 (1961).

14. G. T. Trammell, Phys. Rev. 92, 1387 (1953).

15. G. Bacon, Neutron Diffraction (Oxford University Press, London, 1962).

16. J. J. Sakurai, Advanced Quantum Mechanics (Addison-Wesley Publishing Company, Inc., Reading, Massachusetts, 1967).

17. C. Kittel, Introduction to Solid State Physics (Wiley, New York, 1966).

18. J. C. Slater, Phys. Rev. 51, 846 (1937).

19. D. D. Koelling, J. Phys. Chem. Solids 33, 1335 (1972).

20. T. Loucks, Augmented Plane Wave Method (W. A. Benjamin, Inc., New York, 1967).

21. L. F. Mattheiss, J. H. Wood, and A. C. Switendick, Methods in Computational Physics (Academic Press, New York, 1968), Vol. 8.

22. W. B. Pearson, A Handbook of Lattice Spacings and Structures of Metals and Alloys (Pergamon Press, Inc., New York, 1958).

23. L. F. Mattheiss, Phys. Rev. 133, A1399 (1964).

24. J. C. Slater, Phys. Rev. 81, 385 (1951).

25. B. N. Harmon and A. J. Freeman, Phys. Rev. B 10, 1979 (1974), and B. N. Harmon, Ph.D. thesis, Northwestern University, 1973 (unpublished).

26. J. D. Jackson, Classical Electrodynamics (John Wiley & Sons, Inc., New York, 1962).

27. H. Schlosser and P. M. Marcus, Phys. Rev. 131, 2529 (1963).

28. W. Marshall and S. W. Lovesey, Theory of Thermal Neutron Scattering (Oxford University Press, London, 1971).

29. M. Rotenberg, R. Bivins, N. Metropolis, and J. K. Wooten, The 3-j and 6-j Symbols (The Technology Press, M.I.T., Massachusetts, 1959).

30. E. V. Condon and G. H. Shortley, The Theory of Atomic Spectra (Cambridge University Press, London, 1951).

31. A. R. Edmonds, Angular Momentum in Quantum Mechanics (Princeton University Press, Princeton, 1960).

32. M. E. Rose, Elementary Theory of Angular Momentum (John Wiley & Sons, Inc., New York, 1957).

33. G. Giiat and L. J. Raubenheimer, Phys. Rev. 144, 390 (1966)

34. G. Lehman and M. Taut, Phys. Stat. Sol. 54, 469 (1972)

35. O. Jepsen and O. K. Andersen, Sol. State Comm. 9, 1763 (1971)

36. J. Rath and A. J. Freeman, Phys. Rev. (to be published).

37. P. A. Lindgard, AEC, Risø, 4000 Roskilde, Denmark. (to be published).

38. L. Ley, S. P. Kowalczyk, F. R. McFeely, and D. A. Shirley, Phys. Rev. B (to be published).

39. A. J. Freeman, B. N. Harmon, and T. J. Watson-Yang, Phys. Rev. Letters (to be published).

40. C. Herring, Magnetism, edited by G. T. Rado and H. Suhl (Academic Press, New York, 1966), Vol. IV.

ACKNOWLEDGMENTS

The author would like to thank his advisor, Professor S. H. Liu for his suggestion of this problem, for his patient guidance, and for his continued encouragement and enthusiasm throughout the completion of this study.

The author would also like to extend his thanks to Professor S. K. Sinha, who saved the author from deep frustration and interested him in the theoretical study. Many conversations with him enlightened the author, and provided insights in many respects of this study.

Very special gratitude and appreciation are given to Dr. B. N. Harmon for his generosity and wisdom during the innumerable number of conversations concerning the details of computational and theoretical aspects of the present work.

Finally, the author wishes to express his deepest thanks to his parents, to his brothers and sisters, and to his wife for their encouragement and understanding throughout the entire period of his study.

APPENDIX

In the following, we give a proof that there are no q^{-1} divergent terms in χ in Eq. (31) as q approaches zero. The collection of the q^{-1} divergent terms (T) in Eq. (31) can be written as

$$T = \frac{2e^2}{m^2c^2Gq} \sum_{nk} \left[\sum_{n' \neq n} \frac{f_{nk} - f_{n'k}}{E_{n'k} - E_{nk}} - \delta_{nn'} \frac{\partial f_{nk}}{\partial E_{nk}} \right]$$

$$\times \langle n\vec{k}|p_x e^{-iGy}|n'\vec{k}\rangle \langle n'k|p_x|n\vec{k}\rangle$$

$$- \frac{2e^2}{mc^2Gq} \sum_{nk} f_{nk} \langle n\vec{k}|e^{-iGy}|n\vec{k}\rangle \qquad (A.1)$$

If we use the identity

$$\langle n'\vec{k}|\vec{p}|n\vec{k}\rangle = \frac{im}{\hbar} (E_{n'k} - E_{nk}) [\langle n'\vec{k}|\vec{r}|n\vec{k}\rangle + i\langle n'\vec{k}|\nabla_k(n\vec{k})\rangle]$$

$$+ \frac{m}{\hbar} \delta_{nn'} \nabla_k E_{nk}, \qquad (A.2)$$

Eq. (A.1) becomes

$$T = \frac{2ie^2}{\hbar mc^2Gq} \sum_{nk} \sum_{n' \neq n} (f_{nk} - f_{n'k}) \langle n\vec{k}|p_x e^{-iGy}|n'\vec{k}\rangle$$

$$\times [\langle n'\vec{k}|x|n\vec{k}\rangle + i\langle n'\vec{k}|\frac{\partial}{\partial k_x}(n\vec{k})\rangle]$$

$$- \frac{2e^2}{\hbar mc^2 Gq} \sum_{nk} \frac{\partial f_{nk}}{\partial E_{nk}} \nabla_k E_{nk} \langle n\vec{k} | p_x e^{-iGy} | nk \rangle$$

$$- \frac{2e^2}{mc^2 Gq} \sum_{nk} f_{nk} \langle n\vec{k} | e^{-iGy} | nk \rangle \qquad (A.3)$$

$$= \frac{2ie^2}{\hbar mc^2 Gq} \sum_{nk} f_{nk} \langle n\vec{k} | [p_x e^{-iGy}, x] | n\vec{k} \rangle$$

$$- \frac{2e^2}{\hbar mc^2 Gq} \sum_{nk} f_{nk} \frac{\partial}{\partial k_x} \langle n\vec{k} | p_x e^{-iGy} | n\vec{k} \rangle$$

$$- \frac{2e^2}{\hbar mc^2 Gq} \sum_{nk} \frac{\partial f_{nk}}{\partial k_x} \langle n\vec{k} | p_x e^{-iGy} | n\vec{k} \rangle$$

$$- \frac{2e^2}{mc^2 Gq} \sum_{nk} f_{nk} \langle nk | e^{-iGy} | nk \rangle \, . \qquad (A.4)$$

The first and the last terms cancel each other when we use $[p_x e^{-iGy}, x] = \frac{\hbar}{i} e^{-iGy}$, and the sum of the second and third terms can be transformed easily into a surface integral

$$- \frac{2e^2}{\hbar mc^2 Gq} \sum_{n} \int \frac{dk_y dk_z}{(2\pi)^3} f_{nk} \langle n\vec{k} | p_x e^{-iGy} | n\vec{k} \rangle \Big|_{k_x = \text{zone boundary}}$$

This is zero because

$$\langle n\vec{k} | p_x | n\vec{k} \rangle = \frac{m}{\hbar} \nabla_{k_x} E(\vec{k}) \qquad (A.2')$$

and $\nabla_{k_x} E(\vec{k}) = 0$ at the k_x zone boundary.